UNIVERSITY OF ICELAND

MSc Thesis
in Theoretical Physics

False Vacuum Decay Seeded by Global Cosmic Strings

Phoebe Richman-Taylor

January 2026

FACULTY OF PHYSICAL SCIENCES

False Vacuum Decay Seeded by Global Cosmic Strings

Phoebe Richman-Taylor

Thesis submitted in partial fulfillment of a
Masters of Science degree in Theoretical Physics

M.S. Committee
Florian Niedermann
Aleksandr Chatrchyan
Jesús Zavala Franco

Examiner
Bibhushan Shakya

Faculty of Physical Sciences
School of Engineering and Natural Sciences
University of Iceland
Reykjavik, January 2026

False Vacuum Decay Seeded by Global Cosmic Strings

()

60 ECTS
Thesis submitted in partial fulfillment of a *MSc* degree in Theoretical Physics

Faculty of Physical Sciences
School of Engineering and Natural Sciences
University of Iceland
Dunhagi 5
107 Reykjavik
Iceland

Telephone: 525-4000

Bibliographic information:
Phoebe Richman-Taylor, 2026, *False Vacuum Decay Seeded by Global Cosmic Strings*, MSc-Thesis, Faculty of Physical Sciences, University of Iceland, 61 pp.

Reykjavik, Iceland, January 2026

Abstract

A complex scalar field caught in the false minimum of a potential may tunnel through the potential barrier and create a bubble expanding and converting all of space into the true vacuum. This phenomenon introduced by S. Coleman and C. Callan is reviewed with great care and then expanded upon. We consider a vacuum state containing a straight, global or local cosmic string. The core is occupied by the true vacuum which is separated by a thin cylindrical wall from the false vacuum in the exterior of the string core. This setup is modeled by a complex scalar field under a global or local U(1) symmetry with non-zero winding with a wine bottle potential of nearly degenerate minima. We compute the bounce action for a global-string-induced tunneling, where the string is destabilized locally developing an expanding lump that converts space into the true vacuum. This new bounce configuration has an O(2) x O(2) symmetry. We solve the bounce and the solution is then used to model the shape and trajectory of these elongated bubbles for a full range of parameter values. We compare the string induced tunneling to that of the Coleman bubble and describe the parameter range where the cosmic string bubbles dominate the transition rate.

Dedication

This thesis is dedicated to my beloved companions Poppy and Steve Richman-Taylor.

Figure 0.1. Right hand image depicts the esteemed Poppy while the left hand depicts the infamous Steve.

Table of Contents

List of Figures

List of Tables

Abbreviations

TWL Thin Wall Limit

GW Gravitational Wave

CMB Cosmic Microwave Background

EOM Equations of Motion

Acknowledgements

This thesis was completed with help from supervisors Florian Niedermann and Aleksandr Chatrchyan, I am grateful for all the advice and revisions. Support was provided by the University of Iceland and Erasmus+ project number 2025-1-IS01-KA131-HED-000317721.

1 Introduction

The decay of the false vacuum is described by the "Bounce" solution, studied in [1, 2] by S. Coleman and C. Callan. The solution considers a metastable Lorentz invariant vacuum, has O(4) symmetry and results in an expanding spherical bubble converting all space to the true vacuum as shown in Figure 1.1. The phase transition in this scenario provides an exciting footing for exploration of many topics. The transition to a lower energy potential would in theory inject some energy into the vacuum, this is a particularly interesting effect and has applications for well motivated physics beyond the standard model. Vacuum decay in a first-order phase transition is also relevant for many current cosmological problems. For example it can be applied to Baryogenesis [3], the production of dark matter [4, 5] and maybe even the Hubble tension [6]. The vacuum bubbles could also produce as stochastic background of Gravitational Wave (GW) when they collide [7].

Our setup assumes the existence of cosmic strings (not to be confused with Cosmic Superstrings originating from string theory [8, 9]). These are a non-trivial field solution which introduce a complex phase with a winding number [10]. With such a phase there exists a point in the field profile where the phase becomes degenerate leaving a one dimensional singularity, the cosmic string. They are incredibly interesting in their various effects, possibly leaving signals in the Cosmic Microwave Background (CMB) and possibly having some seeding effect on matter overdensities [11–13]. Cosmic strings are a somewhat contentious area of research as time and time again we have failed to isolate any of the predicted signals they might have produced. Our mechanism offers a way for the strings to have existed and, ease conflict with the current observations.

Our research considers the effects on vacuum decay when a string is present. This translates to our setting of a U(1) complex scalar field in a potential containing a true and false minimum. Further, assuming a nearly negligible energy difference simplifies the analysis. The shape and requirements of our potential are described in detail in Section 1.1. Seeded vacuum decay is a rich area of research where many different sources for vacuum bubbles forming have been studied. In [14–21] authors considered black holes as seeds for vacuum decay. Monopoles as an enhancement for phase transitions are studied in [22–25]. The domain wall as a source for phase transitions is studied in [26–28].

We consider the vacuum decay rate when we no longer have a Lorentz invariant vacuum and instead have some classically stable symmetry breaking object, a cosmic string with $O(2)$ symmetry. For simplicity we assume a sextic potential that maintains the classical stability of the system and allows for metastable cosmic strings. We consider the case where the cosmic string transitions to an unstable solution via sub-barrier tunneling and expands radially at relativistic speeds, restoring the symmetry of the vacuum to that of the Lorentz invariant vacuum; ultimately making itself disappear.

The main objective of this work is to compute the lifetime of a metastable vacuum as defined by our potential. While this has been initially attempted in the literature [29, 30], we for the

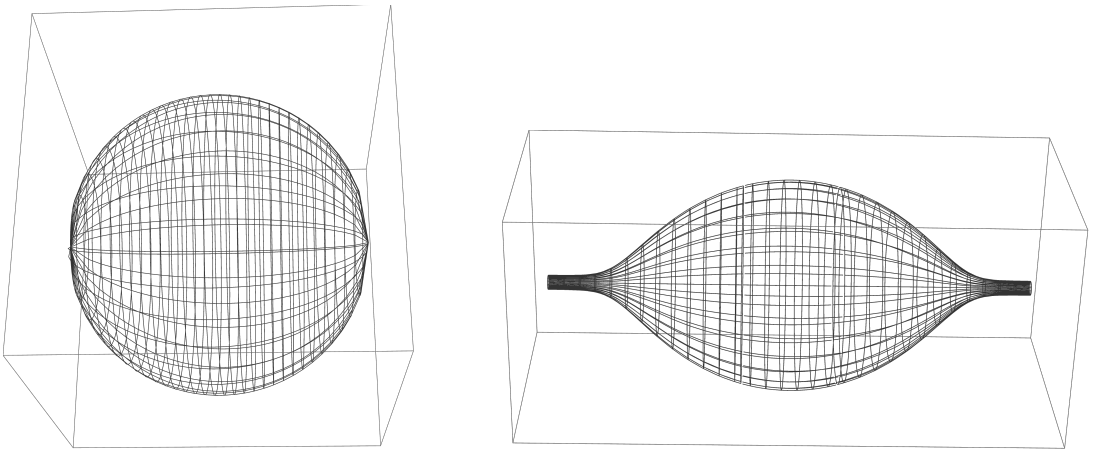

Figure 1.1. The left image shows the $O(4)$ and $O(3) \times \tau$ bounce solutions and the right shows the $O(2) \times O(2)$ solution.

first time provide a result that fully covers the parameter space in the so-called Thin Wall Limit (TWL), and takes into account relativistic corrections. This enables us to describe in which parameter regime the false vacuum decays through this new process and where it proceeds through conventional Coleman bubble nucleation. Moreover, we can study the dynamics of the bubbles after the phase transition has begun.

Let us start by providing an outline of this thesis: In Section 2 we draw a connection between single particle quantum tunneling and tunneling in field theory. We show that the tunneling rate can be written as the exponential of the Euclidian action of the bounce. We then review the tunneling amplitude in an O(4) symmetric case with a scalar field ϕ. We introduce the TWL to get the final Euclidian action found in [1, 2]. We next give and alternative derivation where we assume only $O(3)$ symmetry and then apply a Lorentz boost to the static wall profile to propagate through time. We recover the same result as in the $O(4)$ case, an important equivalence that we make use of in Section 4. Finally, we explicitly show that the TWL allows us to ignore the friction term in the Equations of Motion (EOM) of the field in the wall region.

In Section 3 we consider the static and straight cosmic string with $O(2)$ symmetry. The section explores the differences between global and local symmetry arising from our cosmic string. We evaluate the EOM for cosmic strings in our given symmetry and potential, then explore the radial profile of a string that is estimated to have negligible wall width, making it effectively a hollow cylinder, all expressed in terms of the winding number n. We discuss the validity of the TWL for cosmic strings. Finally we have a very brief discussion of possible observable signals that may be caused by cosmic strings.

Section 4 is the main part of this work. Here we consider the TWL in our new global $O(2) \times O(2)$ symmetry and show that the EOM can again be simplified in the wall region. We compute the generalized bounce solution depicted in the right panel of Figure 1.1, which illustrates the physical decay of the false vacuum seeded by a cosmic string. This in turn allows us to compute the Euclidian action, which controls the tunneling rate. We then show that when the effective winding number approaches 0 we recover the result from the $O(4)$ case in Section 2. We compute the action numerically to show the wall profile and tunneling probability of our expanding string under the full range of parameter values. We consider the dynamics of the string wall and show that the velocity is never superluminal—an important

consistency check. Finally we discuss the phenomenology and compare the lifetimes of vacuums containing cosmic strings and those which only decay via Coleman tunneling. The main results of this thesis are an explicit expression of the $O(2) \times O(2)$ bounce action whose solution is described in Figure 4.6, the radial profile of an expanding local cosmic string found in Figure 4.8, the velocity profile of the bubble wall found in Figure 4.12 and the regime of validity for which the string solution dominates nucleation (233). The contents of this can in part be found in our recent preprint [31] not including the wall velocity discussion. The paper contains a detailed discussion of GW produced by the local string decay and a cosmological model leading to a universe where this decay mechanism is viable. Neither of these discussions are included in this thesis. Our analysis takes $\hbar = c = 1$ and our sign convention is (-,+,+,+).

1.1 Setup

Throughout this thesis we explore false vacuum tunneling. We would therefore like to begin by defining the corresponding potential that admits this false vacuum. Moreover instead of a real scalar field we have a complex scalar field with global or local U(1) symmetry. We require the presence two minima with one lower than the other, the lower is the true vacuum while the higher is the false vacuum. For a complex scalar field this points to a sextic potential, which we can write in its most general form as

$$V(|\phi|) = V_1 + \mu^2|\phi|^2 - \lambda|\phi|^4 + \lambda_6|\phi|^6. \tag{1}$$

Our potential is required to exhibit 2 minima, the true minimum lying at $|\phi_0|$=0 and the false minimum lying at $|\phi_f|$. An action must be dimensionless and the potential V thus has four mass dimensions. We can then infer the following dimensions

$$[V_1] = 4, \;\; [|\phi|] = 1, \;\; [\mu] = 1, \;\; [\lambda] = 0, \;\; [\lambda_6] = -2. \tag{2}$$

We can find some limits on the coefficients λ, λ_6 and μ by imposing our shape requirements. First we look for the extrema of our potential by requiring

$$V'(|\phi|) = 2\mu^2|\phi| - 4\lambda|\phi|^3 + 6\lambda_6|\phi|^5 = 0. \tag{3}$$

The first trivial root lies at $|\phi_0|$=0 as we desired initially. The other two are

$$|\phi|^2 = \frac{2\lambda \pm \sqrt{(2\lambda)^2 - 12\lambda_6\mu^2}}{6\lambda_6} \rightarrow |\phi_f|^2 = \frac{2\lambda + \sqrt{(2\lambda)^2 - 12\lambda_6\mu^2}}{6\lambda_6}, \tag{4}$$

Where the "-" branch corresponds to a local maximum and the "+" branch to a local minimum which we identify with our described false vacuum at $\phi = \phi_f$. We know that $|\phi| \in \mathbb{R}$ and we therefore require the argument of the root in (4) to be greater than or equal to 0. This provides our first bound

$$0 < 4\lambda^2 - 12\lambda_6\mu^2 \Rightarrow \frac{1}{3} > \frac{\lambda_6\mu^2}{\lambda^2}. \tag{5}$$

Next, we impose a lower bound by requiring

$$V(0) < V(|\phi_f|).$$

This translates to

$$V_1 < V_1 + \mu^2|\phi_f|^2 - \lambda|\phi_f|^4 + \lambda_6|\phi_f|^6. \tag{6}$$

This is the condition that ϕ_f is indeed a false minimum. We can input $|\phi_f|^2$ from (4) to find

$$0 < \mu^2 - \lambda\left(\frac{\lambda + \sqrt{\lambda^2 - 3\lambda_6\mu^2}}{3\lambda_6}\right) + \lambda_6\left(\frac{\lambda + \sqrt{\lambda^2 - 3\lambda_6\mu^2}}{3\lambda_6}\right)^2, \tag{7}$$

which expands to

$$0 < \mu^2 - \lambda\left(\frac{\lambda + \sqrt{\lambda^2 - 3\lambda_6\mu^2}}{3\lambda_6}\right) + \frac{1}{9\lambda_6}\left(\lambda^2 + 2\lambda\sqrt{\lambda^2 - 3\lambda_6\mu^2} + \lambda^2 - 3\lambda_6\mu^2\right). \tag{8}$$

We multiply the inequality by $9\lambda_6$ and then combine terms to find

$$0 < 6\mu^2\lambda_6 - \lambda^2 - \lambda\sqrt{\lambda^2 - 3\lambda_6\mu^2}. \tag{9}$$

We divide everything by λ^2 and rearrange, giving

$$\sqrt{1 - \frac{3\lambda_6\mu^2}{\lambda^2}} < \frac{6\mu^2\lambda_6}{\lambda^2} - 1. \tag{10}$$

We next square both sides and combine like terms after factoring out $\frac{\lambda_6\mu^2}{\lambda^2}$ we obtain

$$\frac{1}{4} < \frac{\mu^2\lambda_6}{\lambda^2}. \tag{11}$$

We now have explicit bounds on the shape of our potential. To be explicit, combining with (5), we find

$$\frac{1}{4} < \frac{\mu^2\lambda_6}{\lambda^2} < \frac{1}{3}. \tag{12}$$

Throughout our analysis we write our potential in a more digestible form

$$V(|\phi|) = \lambda_6\left(|\phi|^2 - v_f^2\right)^2\left(|\phi|^2 - \varepsilon v_f^2\right). \tag{13}$$

Where we introduced our vacuum expectation value $|\phi_f| = v_f$. Referring to (1), we chose our V_1 term such that $V(|\phi_f|) = 0$, our value ε is assumed to be small. In fact, we will use it as a dimensionless smallness parameter to realize what is called the thin-wall potential, which is characterized by two almost degenerate minima. This will often allow us to drop terms of order ε. To relate the potential in (1) to the simpler form above, we use the identities

$$\varepsilon = -2 + \frac{\lambda(4\lambda - 3\lambda_6 v_f^2)}{2\lambda_6\mu^2}, \qquad [\varepsilon] = 0, \tag{14}$$

and

$$v_f^2 = \frac{2}{3\lambda_6}\left(\lambda + \sqrt{\lambda^2 - 3\lambda_6\mu^2}\right), \qquad [v_f] = 1. \tag{15}$$

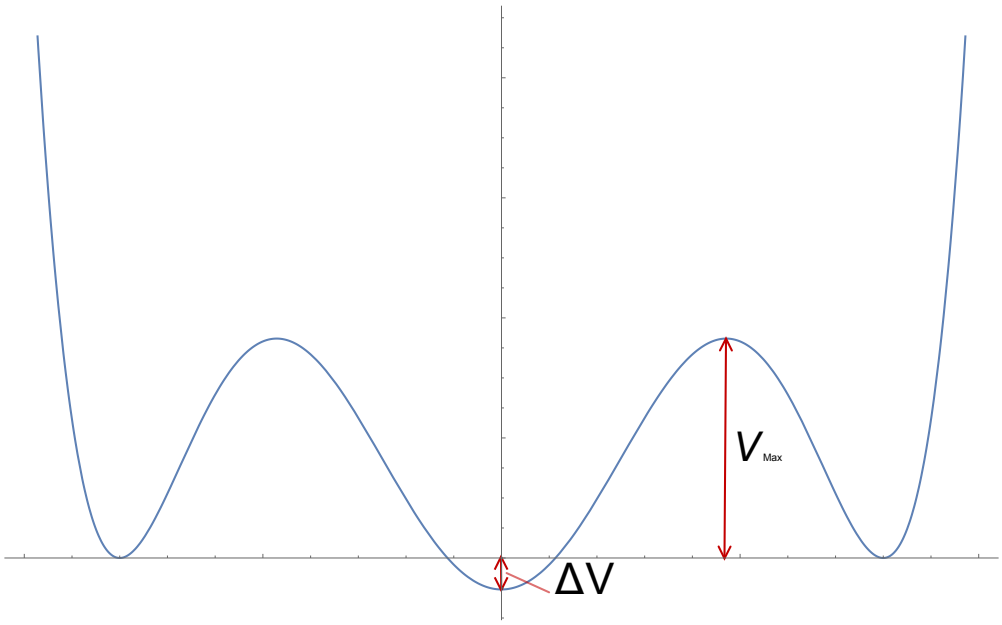

Figure 1.2. The potential $V(|\phi|)$ defined in (13), where ΔV denotes the difference in potential energy between the two minima and V_{Max} the height of the potential barrier.

We can see a 2D projection of the shape of our potential in Figure 1.2. We will find the quantities highlighted to be useful in future computations regarding our discussion of the thin-wall limit. We have taken $\frac{\bar{v}_f}{\sqrt{2}} = v_f$ Our potential is now written

$$V(|\phi|) = \frac{\lambda_6}{8}(2|\phi|^2 - \bar{v}_f^2)^2(2|\phi|^2 - \varepsilon\bar{v}_f^2). \tag{16}$$

We drop the "-" from notation for the rest of this thesis. Currently we would like to introduce the energy density difference between the true and false vacuums

$$|V(0)| = \Delta V = \frac{\varepsilon\lambda_6 v_f^6}{8}. \tag{17}$$

The expression for V_{Max} can be found by evaluating our potential $V(|\phi_{Max}|)$ for the "-" branch in (4). Using the definitions in (14) and (15) we find

$$|\phi_{Max}| = v_f\sqrt{\frac{1+2\varepsilon}{3}}. \tag{18}$$

We can then explicitly compute the height of our potential barrier to be

$$V_{Max} = V(|\phi_{Max}|) = \frac{\lambda_6}{8}\left(\frac{v_f^2(1+2\varepsilon)}{3} - v_f^2\right)^2\left(\frac{v_f^2(1+2\varepsilon)}{3} - \varepsilon v_f^2\right)$$
$$= \frac{\lambda_6 v_f^6}{54} + O(\varepsilon). \tag{19}$$

We would lastly like to compare the height of the potential barrier V_{Max} to the difference ΔV to see

$$\frac{\Delta V}{V_{Max}} = \frac{\varepsilon \lambda_6 v_f^6}{8} \frac{54}{\lambda_6 v_f^6} \sim \varepsilon. \tag{20}$$

We have built our potential with the distinct choice of ε to be small, thus our result tells us that the energy difference between the true and false vacuum is negligible with respect to the height of the potential barrier. This result is useful for our future computations.

The potential $V(|\phi|)$ is invariant under a general U(1) transformation:

$$\phi \to \phi e^{i\alpha(x)}. \tag{21}$$

This follows from the fact that $V(|\phi|)$ only depends on $|\phi|$ and $|\phi| \to \sqrt{\phi e^{i\alpha(x)} \phi e^{-i\alpha(x)}} = |\phi|$, thus $V(\phi) = V(\phi e^{i\alpha(x)})$. We refer to this as local U(1) if $\alpha(x)$ has a spatial dependence. On the other hand if $\alpha = const$ then we have global $U(1)$ symmetry. In the global case we need some gauge potential A_μ to make the kinetic term invariant.

1.2 Introducing the Cosmic String Induced Tunneling Topic

Let us review the previous works published on the vacuum phase transition seeded from a cosmic string bubble. The first mention of this problem was in [32] where the authors consider both monopoles and cosmic strings. We will focus only on the cosmic string perspective. Here the authors consider the effects of the spacetime distortion caused by such a topological defect. The authors introduce a factor C which corresponds to the angle deficit $\delta = 8\pi G\mu_s$ due to the string tension μ_s and neglect the string winding, more specifically they assume an O(4) symmetry despite the presence of a string. The bounce solution (a modified action), in this case is found to be

$$B_s = \frac{27\pi^2 \sigma^4 C_s^2}{2\Delta V^3}, \tag{22}$$

where $C_s^2 = 1 - \frac{\delta}{2\pi} = 1 - 4G\mu_s$. We see that the formula recovers the result in [1] in the limit ($\delta << 1$). The angle deficit is found to result in an enhanced tunneling rate but only very slightly larger than the Coleman vacuum tunneling scenario. The reason for this limit is that in general $\delta = 8\pi G\mu_s < 1$ for cosmic strings in standard GUT scale scenarios. The authors introduce the lifetime of a vacuum containing a cosmic string to be

$$T_s = \frac{1}{L_s V \Gamma_s} = L_s^{-1} V^{-1} m^{-2} e^{-B_s} \tag{23}$$

where L_s refers to the average length of string contained per volume V, Γ_s is the tunneling rate per string length and m is the typical mass scale of the tunneling sector. Their analysis has several limitations: (i) They neglect that the bounce has $O(2) \times O(2)$ symmetry and instead choose to evaluate under $O(4)$ symmetry. (ii) They employ an expression for the deficit angle δ, that is only valid outside of the string. (iii) They focus on the case with a very small effect

by choosing $\delta << 1$. Later we will see that (i) is only justified in the particular limit where the string is infinitely thin.

The problem is also discussed in [30] in the local symmetry case. This work considers a wine bottle potential, however, it is not specified to be in the thin-wall limit. In the same work the cases of finite temperature and zero temperature potentials are explored, where zero temperature is of greatest interest for our work. Moreover they focus on the unit winding case. The work proves the existence of an $O(2) \times O(2)$ symmetric bounce solution but does not explicitly compute it.

This idea was left nearly untouched until 2013 where the subject was explored further in [29]. Here the author considers the local string case. An important limitation of this paper is that the bubble expansion is assumed to be non-relativistic in the computation of the Euclidian action. The authors define the field ansatz to have general winding number n and they perform a numerical shooting algorithm to find a final solution for the bubble profile. While our work will follow their technical strategy we will go beyond the limit of non-relativistic wall velocities. Moreover, we will provide an analysis of the whole parameter space in the thin-wall limit. We will also specifically work out the parameter limit that allows us to recover the results of [29].

A similar setup is discussed in [33] where the authors consider vortices in type-II superconductors which are similar to cosmic strings. There the winding number is chosen to be $n > 1$ in contrast to our $n \geq 0$. The thick wall case is also discussed as well as the parameter ε related to the potential energy difference between the two minima. There is a great discussion of such limits on ε so that the string remains classically stable.

There are more modes of decay for cosmic strings, for example formation of a monopole and anti-monopole pair as discussed in [34–36] where they relate the distance between the pair of particles to the radius of a vacuum bubble. This relation between the two symmetries provides another example in calculating the bounce action, however, it constitutes a different physical scenario and relies on the viability of magnetic monopoles.

2 Simple Quantum Tunneling

2.1 1D Quantum Tunneling

We would like to first consider the simplest possible example of quantum tunneling, that is 1D tunneling as discussed in [37]. We will consider the case of a single particle moving along one dimension traveling through a potential barrier from one false minimum to a lower true minimum. Our tunneling probability is written as

$$\Gamma = Ae^{-B/\hbar}(1+O(\hbar)). \tag{24}$$

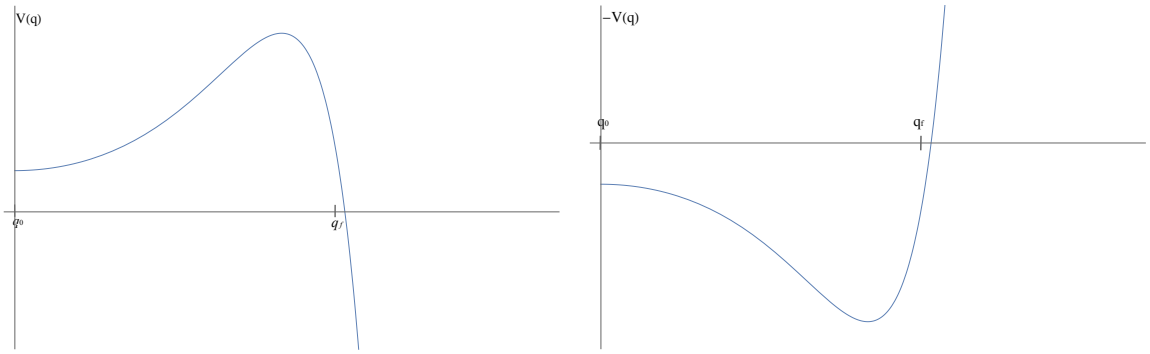

Figure 2.1. A basic potential for the simple 1D tunneling. The left plot shows the potential in real time t and the right side shows the upside-down potential in Euclidian time τ. The point q_0 is the start and end point for the particle and the point q_f is the turnaround point assuming energy is conserved.

The standard result in QM tunneling discussion is

$$B = \int_{q_0}^{q_f} dq\sqrt{2(V(q)-E)}, \tag{25}$$

where q_0 is the starting position of the particle and q_f is the end point at which the particle exits the classically forbidden region. We will connect these well known results to the field theory case such that our future computations have a simple basis. We do this by expressing B in the form of the Euclidian action. This equivalence is useful in the field theory computation as it eliminates the need for defined endpoints. We first consider the lagrangian

$$L = \frac{1}{2}\left(\frac{dq}{dt}\right)^2 - V(q), \tag{26}$$

and EOM

$$\frac{d^2q}{dt^2} + \frac{V(q)}{dq} = 0, \tag{27}$$

for our 1D particle. We have chosen q to represent a position along the potential and t real time. At this point we make the key transformation of real time into Euclidian time, that is $\tau = it$ which gives a new EOM of the form

$$\frac{d^2q}{d\tau^2} - \frac{V(q)}{dq} = 0. \tag{28}$$

Obtained from the following Euclidian Lagrangian

$$L_E = \frac{1}{2}\left(\frac{dq}{d\tau}\right)^2 + V(q). \tag{29}$$

This is now the EOM with a flipped potential, shown in Figure 2.1. We proceed to define our boundary conditions for our particle. The setup begins with a particle that is at some early time placed very near to the top of a hill ($q(\tau)|_{\tau\to-\infty} = q_0$), where after a very long time it begins to roll down the hill and then up the next slope and after some time ($q(0) = q_f$), there it stops $\left(\frac{dq}{d\tau}\big|_{\tau=0} = 0\right)$ and turns around then rolls back up its original hill such that after a very long time it reaches its starting point again ($q(\tau)|_{\tau\to\infty} = q_0$). This listed set of boundary conditions constitutes the “Bounce" solution. Let us observe what happens in the formulation of (25) with our new bounce conditions. Our total energy is written

$$E = \frac{1}{2}\left(\frac{dq}{dt}\right)^2 + V(q) = L + 2V(q). \tag{30}$$

We can choose $E = 0$ for convenience and define that at position q_0 we have $V(q_0) = 0$ and $\frac{dq}{dt}\big|_{q_0} = 0$. This choice, coupled with our definition of total energy (30) provides us with the equality

$$-\frac{1}{2}\left(\frac{dq}{dt}\right)^2 = \frac{1}{2}\left(\frac{dq}{d\tau}\right)^2 = V(q). \tag{31}$$

We can now re-write our bounce starting from (25)

$$\begin{aligned} B = 2\int_{q_0}^{q_f} dq\sqrt{2V} = 2\int_{q_0}^{q_f} dq\frac{dq}{d\tau} = \int_{-\infty}^{\infty} d\tau\left(\frac{dq}{d\tau}\right)^2 \\ = \int_{-\infty}^{\infty} d\tau\left[\frac{1}{2}\left(\frac{dq}{d\tau}\right)^2 + V(q)\right] = \int_{-\infty}^{\infty} d\tau L_E = S_E, \end{aligned} \tag{32}$$

we have applied our choice of $E = 0$ and taken our Euclidian definition from (31). Our factor of 2 is absorbed when we adjust the limits to those of τ. Our relation shows that B, and thus the tunneling probability, can be expressed with the Euclidian action evaluated for the bounce solution. This result was then generalized by Coleman [1] to the field theoretic case, where the tunneling probability is controlled by the Euclidian action. We discuss this derivation in the next section.

2.2 The Coleman Bubble

We would now like to generalize our problem to that of a trapped complex scalar field. We consider the case of three spatial dimensions, a time dimension and the false vacuum potential

described in Section 1.1. We will compute the bounce action for our field configuration. Throughout the entirety of this thesis we are interested in the bounce solutions thus with any mention of the 'Bubble' the bounce is implied. We are interested in bubble configurations, which look the same when approached from any spatial or time axis. Inside the sphere the field lies in the true vacuum and outside of this sphere the field is in the false vacuum. We begin by introducing our field and Lagrangian followed by defining our coordinate system and then computing our EOM. We will introduce the TWL and finally conclude by computing our action.

Our Lagrangian density for the system of interest is written with a complex scalar field ϕ and a vector potential field A_μ. Our field ϕ is symmetric under U(1) transformation, that is to say invariant under $\phi \to \phi e^{i\alpha}$ transformations. Here we have $\mu = [\tau, j]$ and $j = [x, y, z]$,

$$\mathscr{L} = -\frac{1}{4}F^{\mu\nu}F_{\mu\nu} + (D^\mu\phi)^*(D_\mu\phi) - V(|\phi|), \tag{33}$$

where

$$F_{\mu\nu} = (\partial_\mu A_\nu - \partial_\nu A_\mu) \qquad \text{and} \qquad D^\mu = (\partial^\mu + ieA^\mu). \tag{34}$$

Our tensor $F_{\mu\nu}$, the field strength tensor describes the electromagnetic field sourced from our gauge field A_μ. We have our covariant derivative term D^μ which couples the scalar field ϕ to our gauge field A_μ with a coupling constant e. Our global symmetry eliminates any gauge field A_μ and we continue with $A_\mu = 0$ to find

$$\mathscr{L} = (\partial^\mu\phi)^*(\partial_\mu\phi) - V(|\phi|). \tag{35}$$

We have the EOM

$$\frac{d}{dx^\mu}\frac{\partial\mathscr{L}}{\partial(\partial_\mu\phi)} - \frac{\partial\mathscr{L}}{\partial\phi} = 0, \tag{36}$$

$$\frac{d}{dx^\mu}\partial_\mu\phi - \frac{dV}{d\phi} = 0, \tag{37}$$

$$\partial_\tau^2\phi + \partial_j^2\phi = \frac{dV}{d\phi}. \tag{38}$$

We write a new set of conditions that reflect our higher dimensionality and new field ϕ. The first denotes a symmetry of the trajectory centered at $\tau = 0$ and the second imposes a limit such that the action is finite,

$$\frac{\partial\phi}{\partial\tau}\Big|_{\tau=0} = 0 \qquad \text{and} \qquad \lim_{\tau\to\pm\infty}\phi = \phi_f. \tag{39}$$

Similarly, we designate a coordinate in position space for a turnaround point. We will expect the field to have a symmetric spatial profile reflected over the center of symmetry. We choose the position at which we find this symmetry to be $x, y, z = 0$. This position can be chosen to be anywhere so long as it is a center of symmetry, we pick 0 as it simplifies our future computations. We need to identify the bounce conditions of ϕ again to assure a finite action. We write

$$\frac{\partial \phi}{\partial x_i}\Big|_{x_i=0} = 0 \qquad \text{and} \qquad \lim_{x_i \to \pm\infty} \phi = \phi_f. \tag{40}$$

Our action is then written as

$$S = \int d^4x[(\partial^\mu \phi^*)(\partial_\mu \phi) - V(|\phi|)]. \tag{41}$$

We are particularly interested in the thin wall bubble. We have included a small difference of ε in our potential as described in (16) to create a lower well centered at 0 with a difference in potential of (17). With our potential, the action becomes

$$S = \int d^3x dt[(\partial^\mu \phi^*)(\partial_\mu \phi) - \frac{\lambda_6}{8}(2|\phi|^2 - \varepsilon v_f^2)(2|\phi|^2 - v_f^2)^2]. \tag{42}$$

We are interested in the Euclidian action as it simplifies our computations. To convert the action we take our change of variable $t = i\tau$ to obtain S_E. As discussed in the previous subsection the change to Euclidian time results in a flipped potential. We have chosen the notation $\partial_\tau \phi = \dot{\phi}$

$$S = iS_E = i\int d^3x d\tau[\dot{\phi}^*\dot{\phi} + (\partial^j \phi^*)(\partial_j \phi) + \frac{\lambda_6}{8}(2|\phi|^2 - \varepsilon v_f^2)(2|\phi|^2 - v_f^2)^2]. \tag{43}$$

We make an ansatz for the complex scalar field ϕ such that we can separate the amplitude and phase θ with winding number n.

$$\phi(\tau,x,y,z,\theta) = \frac{v_f}{\sqrt{2}} f(\tau,x,y,z)e^{in\theta} \underset{n=0}{\to} \frac{v_f}{\sqrt{2}} f(\tau,x,y,z) \tag{44}$$

In our spherical symmetry the winding contribution disappears. A connected path over the surface of the sphere can be shrunken down continuously to a point, still on the surface. We find

$$S_E = \int d^3x d\tau \left[\frac{v_f^2}{2}\dot{f}^2 + \frac{v_f^2}{2}(\partial_j f)^2 + \frac{\lambda_6 v_f^6}{8}(f^2 - \varepsilon)(f^2 - 1)^2\right], \tag{45}$$

with a potential in the new form

$$V(f) = -\frac{\lambda_6 v_f^6}{8}(f^2 - \varepsilon)(f^2 - 1)^2. \tag{46}$$

With our boundary conditions in (39) and (40) it is logical to combine all the coordinates to a new coordinate $\rho_4 = \sqrt{\tau^2 + x^2 + y^2 + z^2}$ such that our field exclusively depend on this new variable ρ_4 as $f(\rho_4)$. Our boundary conditions now specify the potential in the false vacuum to be $V(1) = 0$ and the potential inside the core under the the TWL to be $-\Delta V$ from (17) (this is the case for real time t with the un-flipped potential as found in (16)). The boundary conditions become

$$\frac{\partial f}{\partial \rho_4}\Big|_{\rho_4=0} = 0 \qquad \text{and} \qquad \lim_{\rho_4 \to \infty} f = 1. \tag{47}$$

We compute the EOM in our simplified coordinate system. We can apply a 4D spherical coordinate change to (45) and gain a factor of $2\pi^2$ to get

$$S_E = 2\pi^2 \int_0^\infty d\rho_4 \underbrace{\rho_4^3 \left(\frac{v_f^2}{2} f'^2 + \frac{\lambda_6 v_f^6}{8} (f^2 - \varepsilon)(f^2 - 1)^2 \right)}_{\mathscr{L}}, \tag{48}$$

where now $f' = \frac{df}{d\rho_4}$. Our EOM takes form

$$\frac{d}{d\rho_4} \frac{\partial \mathscr{L}}{\partial f'} = \frac{\partial \mathscr{L}}{\partial f} \tag{49}$$

$$f'' - \frac{1}{v_f^2} \frac{dV}{df} = -\frac{3}{\rho_4} f' \tag{50}$$

On the right hand side we see a friction term, this has the potential to complicate solving the action.

2.3 The Coleman Bubble in the Thin Wall Limit

In our initial EOM (38), by transforming our time to Euclidian time we have flipped the potential (13). Now we are modeling the field as a particle placed very close to the top of a hill allowed to very slowly start to roll. The particle will gain significant speed traveling down the hill and then back up a very slightly shorter adjacent hill where it will come to rest nearly at the top before rolling back down and then up again, finally coming to rest at its initial starting point on the first hill. The friction term $\frac{3}{\rho} \frac{df}{d\rho}$ must be extremely small for this to occur, due to the very slight difference in heights of the hills. We find the TWL from the assumption that $\varepsilon << 1$ and thus the friction in the EOM is negligible in the wall region. The bounce solution setup described requires the particle to take an extremely long time to start rolling, this is analogous to the field profile as we pass through the wall, constant and then very suddenly changing. This is to say the total time for the particle to go from one peak to the other is much greater than the time the particle spends in the valley between them. These conditions will be explicitly checked in the TWL section. For now we can continue to evaluate our action with the EOM neglecting the friction term

$$\frac{v_f^2}{2} \left(\frac{df(\rho}{d\rho} \right)^2 = V(f), \tag{51}$$

the solution to which is

$$f(\rho) = \frac{e^{\rho \frac{1}{2} \sqrt{\lambda_6} v_f^2}}{\sqrt{2 + e^{\rho \sqrt{\lambda_6} v_f^2}}}, \tag{52}$$

where ρ is some general argument.

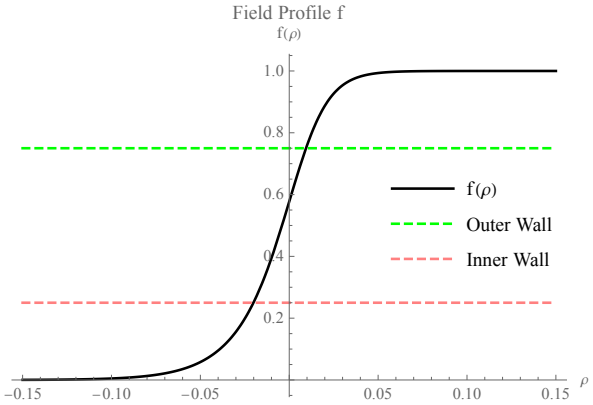

Figure 2.2. The profile field function f as we travel from the true vacuum (left) to the false vacuum (right). The inner and outer wall sit at $f = 1/4$ and $f = 3/4$ respectively.

Continuing with the evaluation of the $O(4)$ action we separate into 3 sections, interior, wall and exterior. S_E^{int} is evaluated first. We have that f and f' are both 0, and the variable ρ_0 is the critical radius at which the bubble will continue expanding. We have

$$S_E^{int} = -\pi^2 \int_0^{\rho_0} d\rho_4 \rho_4^3 \frac{\lambda_6 \varepsilon v_f^6}{4} = -\frac{\pi \rho_0^4 \varepsilon \lambda_6 v_f^6}{16}. \tag{53}$$

For the wall portion we use our definition that $f|_{\rho_4=\infty} = 1$, giving

$$S_E^{wall} = 2\pi^2 \int_{\rho_0-\delta}^{\rho_0+\delta} d\rho_4 \rho_4^3 (v_f^2 \frac{f'^2}{2} + V(f)). \tag{54}$$

We use (51) to combine the two terms and select our definition of the wall tension σ

$$S_E^{wall} = 2\pi^2 \rho_0^3 \underbrace{\int d\rho_4 v_f^2 f'^2}_{\sigma} = 2\pi^2 \rho_0^3 \sigma. \tag{55}$$

The exterior portion of the action is trivially 0 and we thus have

$$S_E = S_E^{int} + S_E^{wall} + S_E^{ext} = -\frac{\pi^2 \varepsilon \rho_0^4 \lambda_6 v_f^6}{16} + 2\pi^2 \rho_0^3 \sigma + 0 = -\frac{1}{2}\pi^2 \rho_0^4 \Delta V + 2\pi^2 \rho_0^3 \sigma, \tag{56}$$

where we have taken the definition from (17) and applied it to (53). We will now explicitly compute the wall tension, starting with our definition of

$$\sigma = \int d\rho_4 v_f^2 f'^2 = v_f \int d\rho_4 \frac{df}{d\rho_4} \sqrt{2V(f)} = v_f \sqrt{2} \int_0^1 df \sqrt{V(f)}. \tag{57}$$

The TWL allows us to explicitly evaluate the wall tension for our potential (46),

$$\sigma = v_f \int_0^1 df \sqrt{2V(f)} = v_f \sqrt{\frac{2\lambda_6 v_f^6}{8}} \int_0^1 df \sqrt{(f^2-\varepsilon)(f^2-1)^2}, \tag{58}$$

finally taking ε to be 0 with

$$\frac{\sqrt{\lambda_6}v_f^4}{2}\int_0^1 df(f-f^3) = \frac{\sqrt{\lambda_6}v_f^4}{2}\left[\frac{1}{2}-\frac{1}{4}\right] = \frac{\sqrt{\lambda_6}v_f^4}{8}. \tag{59}$$

After evaluating we can conclude with the explicit wall tension in the TWL.

$$\boxed{\sigma = \frac{\sqrt{\lambda_6}v_f^4}{8}} \tag{60}$$

We can compute ρ_0 by varying the action (56)

$$\frac{\delta S_E^4}{\delta \rho_0} = -2\pi^2 \Delta V \rho_0^3 + 6\pi^2 \rho_0^2 \sigma = 0. \tag{61}$$

Thus we have

$$\rho_0 = \frac{3\sigma}{\Delta V}, \tag{62}$$

using our definitions for σ and ρ_0. We have the same Euclidian action as was computed in [38]

$$S_E^4 = -\frac{1}{2}\pi^2\left(\frac{3\sigma}{\Delta V}\right)^4 \Delta V + 2\pi^2\left(\frac{3\sigma}{\Delta V}\right)^3 \sigma = \frac{27}{2}\frac{\pi^2\sigma^2}{\Delta V^3}. \tag{63}$$

2.4 The O(3) Symmetric Bubble

The Coleman Bubble we have discussed is O(4) symmetric. We will now explore the effects when we do not assume such perfect symmetry and instead compute our action with time and space separated. Our field still follows a U(1) symmetry and with that a spherical O(3) spatial symmetry. With this, just as in the O(4) case, the gauge field is $A_\mu = 0$. We make the same ansatz for our field ϕ as in (44). From this point forward we will diverge from our previous computations in the O(4) symmetric case.

We can take (45) and apply a spherical coordinate change to the spatial coordinates, we define $r_3 = \sqrt{x^2+y^2+z^2}$. We have $\dot{f}$, f' representing differentiation with respect to the Euclidian time τ and radial coordinate r_3 respectively,

$$S_E^{O(3)} = 4\pi v_f^2 \int_{-\infty}^{\infty} d\tau \int dr_3 r_3^2 \left(\frac{\dot{f}^2}{2} + \frac{f'^2}{2} + \frac{\lambda_6 v_f^4}{8}(f^2-\varepsilon)(f^2-1)^2\right). \tag{64}$$

We must account for relativistic wall speeds in our computations. We make an ansatz for the field function argument by applying a Lorentz boost to the argument of f in the O(4) case. The choice of arguments in f reflects the dependence of the field f on the proximity to the bubble wall specifically as a static wall with a Lorentz boost applied

$$f(\tau, r_3) = f(\underbrace{\gamma(\tau)(r_3 - R(\tau))}_{\zeta(r_3,\tau)}). \tag{65}$$

where

$$\gamma(\tau) = \frac{1}{\sqrt{1+\dot{R}(\tau)^2}}, \tag{66}$$

here $R(\tau)$ is the position of the wall. We have accounted for Lorentz contraction in the wall thickness. The bubble wall is expected to approach relativistic speeds while it expands. We maintain our spherical symmetry and propagate the wall through time resulting in the γ inclusion to maintain Lorentz invariance. Our function f depends only on a single variable ζ as in the O(4) case where it depended only on ρ_4. Our new generalized EOM following our ansatz (65) is

$$v_f^2 \left(\frac{df}{d\zeta}\right)^2 = 2V(f). \tag{67}$$

We can evaluate the $O(3)$ action as in $O(4)$ by evaluating each term in the 3 regions (Inside, Wall, Exterior).

The kinetic term and gradient terms only exist within the wall. When working in this region, we take advantage of our thin wall condition, we can replace any r_3 terms in the spatial derivative with $R(\tau)$ as they behave as constants within this integrand. The same reasoning can be applied when setting any term containing $(r_3 - R(\tau))$ to 0. We find

$$S_{kin}^{O(3)} = 4\pi v_f^2 \int d\tau \int_{R(\tau)-\delta}^{R(\tau)+\delta} dr_3 r_3^2 \frac{\dot{f}^2}{2} = 4\pi v_f^2 \int d\tau R(\tau)^2 \int_{R(\tau)-\delta}^{R(\tau)+\delta} dr_3 \frac{1}{2}\left(\frac{\partial f}{\partial \tau}\right)^2 \tag{68}$$

Applying the chain rule gives

$$\begin{aligned} S_{kin}^{O(3)} &= 4\pi v_f^2 \int d\tau R(\tau)^2 \int_{R(\tau)-\delta}^{R(\tau)+\delta} dr_3 \frac{1}{2}\left(\frac{df}{d\zeta}\right)^2 \left(\frac{\partial \zeta}{\partial \tau}\right)^2 \\ &= 4\pi v_f^2 \int d\tau R(\tau)^2 \int_{R(\tau)-\delta}^{R(\tau)+\delta} dr_3 \frac{1}{2}\left(\frac{df}{d\zeta}\right)^2 (\dot{\gamma}(\tau)(r_3 - R(\tau)) - \gamma(\tau)\dot{R}(\tau))^2. \end{aligned} \tag{69}$$

In the last step we can take advantage of our parametrization and integrate over $d\zeta$ with

$$\gamma(\tau) = \frac{\partial \zeta}{\partial r_3},$$

the change in differential element maintains the same limits and we find

$$S_{kin}^{O(3)} = 4\pi v_f^2 \int d\tau R(\tau)^2 \int_{-\gamma\delta}^{\gamma\delta} d\zeta \frac{1}{2\gamma(\tau)}\left(\frac{df}{d\zeta}\right)^2 (\gamma(\tau)\dot{R}(\tau))^2. \tag{70}$$

We can replace the last integral with the wall tension σ as we defined it in (57)

$$S_{kin}^{O(3)} = 2\pi \int d\tau \gamma R(\tau)^2 \dot{R}^2(\tau)\sigma. \tag{71}$$

The gradient term follows similarly to the kinetic term,

$$S^{O(3)}_{grad} = 2\pi v_f^2 \int d\tau \int_{R(\tau)-\delta}^{R(\tau)+\delta} dr_3 r_3^2 \left(\frac{df}{dr_3}\right)^2$$
$$= 2\pi v_f^2 \int d\tau R(\tau)^2 \int_{R(\tau)-\delta}^{R(\tau)+\delta} dr_3 \left(\frac{\partial f}{\partial \zeta}\right)^2 \left(\frac{d\zeta}{dr_3}\right)^2$$
$$= 2\pi v_f^2 \int d\tau R(\tau)^2 \int_{-\gamma\delta}^{\gamma\delta} \frac{d\zeta}{\gamma} \left(\frac{df}{d\zeta}\right)^2 \gamma^2. \quad (72)$$

We take all our τ dependent terms to the left and find that the $d\zeta$ integration is now exactly σ

$$S^{O(3)}_{grad} = 2\pi v_f^2 \int d\tau \gamma R(\tau)^2 \int_{-\gamma\delta}^{\gamma\delta} d\zeta \left(\frac{df}{d\zeta}\right)^2 = 2\pi \int d\tau \gamma R(\tau)^2 \sigma. \quad (73)$$

The potential term is separated into the inside and wall regions as we defined $f = 0$ inside the bubble and $f = 1$ outside giving the form

$$S^{O(3)}_V = 4\pi \int d\tau \frac{-\lambda_6 \varepsilon v_f^6}{8} \int_0^{R(\tau)-\delta} dr_3 r_3^2 +$$
$$4\pi \int d\tau \int_{R(\tau)-\delta}^{R(\tau)+\delta} dr_3 r_3^2 \frac{\lambda_6 v_f^6}{8} ((f^2-\varepsilon)(f^2-1)^2). \quad (74)$$

We can evaluate the radial integral for the inside region explicitly, for the wall region we use the thinness and choose r_3 to be treated as a constant $R(\tau)$,

$$S^{O(3)}_V = -\frac{\pi \lambda_6 \varepsilon v_f^6}{6} \int d\tau R(\tau)^3 + 4\pi \int d\tau R(\tau)^2 \int_{R(\tau)-\delta}^{R(\tau)+\delta} dr_3 V(f) + O(\delta). \quad (75)$$

We replace the potential in the second term using the EOM we found in (67)

$$S^{O(3)}_V = -\frac{\pi \lambda_6 \varepsilon v_f^6}{6} \int d\tau R(\tau)^3 + 2\pi \int d\tau R(\tau)^2 \int_{-\delta\gamma}^{\delta\gamma} \frac{d\zeta}{\gamma} v_f^2 \left(\frac{df}{d\zeta}\right)^2. \quad (76)$$

We find the wall region then contains the wall tension σ as defined in (57)

$$S^{O(3)}_V = -\frac{\pi \lambda_6 \varepsilon v_f^6}{6} \int d\tau R(\tau)^3 + 2\pi \int d\tau \frac{R(\tau)^2}{\gamma} \sigma. \quad (77)$$

Our final action then follows from combining all the different regions kinetic and potential terms

$$S^{O(3)}_E = -\frac{\pi \lambda_6 \varepsilon v_f^6}{6} \int d\tau R(\tau)^3 + 2\pi \int d\tau \frac{R(\tau)^2}{\gamma} \sigma (1 + \gamma^2 + \dot{R}(\tau)^2 \gamma^2). \quad (78)$$

Simplifying the wall term we find $(1+\gamma^2+\dot{R}(\tau)^2\gamma^2)=2$ and our action becomes

$$S_E^{O(3)} = 4\pi \int d\tau \underbrace{\left(\frac{-\varepsilon v_f^6 \lambda_6}{24} R(\tau)^3 + \frac{R(\tau)^2}{\gamma}\sigma\right)}_{L_E}. \tag{79}$$

We guess a solution of the form,

$$R(\tau) = \sqrt{R_c^2 - \tau^2}, \tag{80}$$

which follows from the O(3) symmetry. This guess solves our EOM

$$\frac{d}{d\tau}\frac{\partial L_E}{\partial(\partial_\tau R)} - \frac{\partial L_E}{\partial R} = 0, \tag{81}$$

which when expanded with the contents of (79) as the langrage L_E gives

$$2R\dot{R}^2\sigma\gamma + R^2\ddot{R}\sigma\gamma - R^2\dot{R}^2\ddot{R}\gamma^3\sigma - (-\Delta V R^2 + 2R\sigma\gamma^{-1}) = 0. \tag{82}$$

From (80) we can compute $\gamma = \frac{R}{R_c}$, $\dot{R} = -\frac{\tau}{R(\tau)}$ and $\ddot{R} = -\frac{1}{R(\tau)} - \frac{\tau^2}{R(\tau)^3}$, giving

$$S_E^{O(3)} = 4\pi \int_{-R_c}^{R_c} d\tau \left(-\frac{\Delta V R(\tau)^3}{3} + R(\tau) R_c \sigma\right). \tag{83}$$

We continue to check that (80) solves (82) and we can proceed to find R_c by first computing the action. We pick limits such that $-R_c < R(\tau) < R_c$ is real giving an action of the form

$$S_E^{O(3)} = 4\pi^2 \left(-\frac{1}{8}R_c^3\right)(\Delta V R_c - 4\sigma). \tag{84}$$

We require that R_c is a critical point in S_E.

$$\frac{\delta S_E^{O(3)}}{dR_c} = 0 = -\frac{1}{2}\pi^2 R_c^2(\Delta V R_c - 3\sigma) \tag{85}$$

We find an explicit value for R_c

$$R_c = \frac{3\sigma}{\Delta V}, \tag{86}$$

solving (82) with (80). We use our R_c combined with (84) and have an explicit value for the bounce

$$S_E^{O(3)} = \frac{\pi^2}{2}\left(27\frac{\sigma^4}{\Delta V^3}\right), \tag{87}$$

coinciding exactly with our result in (63). This is very important for our later computations. We have confirmed that considering a static bubble wall and then applying a Lorentz boost is in fact equivalent to evaluating the bounce action of an $O(4)$ field. This equivalence of approaches between $O(3)\times\tau$ and $O(4)$ is a key part of our later computations of an $O(2)\times O(2)$ symmetric bubble, where we take the approach of applying a Lorentz boost to a static wall.

2.5 The Thin Wall Limit

We will now explicitly show the validity of our TWL approximations. We have choose our potential and bubble configuration such that the field f is constant everywhere except the wall (0 inside and 1 outside) as shown in Figure 2.2. We begin with the assumption that the energy difference between the true and false minimums, ε, is extremely small. In this section we will show that the energy lost due to friction is negligible in the wall region and the thickness of the wall is negligible compared to the radius of the bubble. The entirety of the change in field is inside of the wall, the thinner this wall is the more suddenly this change occurs. We find that the TWL of the EOM is only used while evaluating the action, thus we must only show the suppression of our friction term for the action within the wall region.

We have a potential of the shape (46) and an EOM (67) where f depends exclusively on a variable υ such that $\frac{df}{d\upsilon} = f'$ is a total derivative. We find υ to be a composition of more variables, this is not an issue so long as the field function f is parametrized entirely by υ, whatever υ may be. We have

$$v_f^2 f'' - \frac{dV}{df} = -\frac{3v_f^2}{\upsilon} f'. \tag{88}$$

We consider our trajectory of a single particle again. At some $\tau = -\infty$ we let go and the particle very slowly begins to accumulate speed. When the particle passes the bottom of the well it is moving quickly, as it approaches the top of the next hill it slows until it approaches rest at $\tau = 0$. This suppression can be written as the conditions

$$f'' >> \frac{3}{\upsilon} f' \qquad \text{and} \qquad \frac{dV}{df} >> \frac{3v_f^2}{\upsilon} f'. \tag{89}$$

The stated conditions are more strict than is necessary for our computations, we loosen them by requiring that the inequalities need only be satisfied under integration over the wall region. Concretely, we can show that over the wall region the energy lost due to friction is very small compared to the transfer between kinetic and potential energy as written

$$\int d\upsilon f' (v_f^2 f'' - \frac{dV}{df}) = -\int d\upsilon \frac{3v_f^2}{\upsilon} (f')^2. \tag{90}$$

We have written the EOM (88) in an integration over υ and multiplied a term of f' into both sides that will make the evaluation easier. We prove the validity of the TWL in our method by (i) computing the order of magnitude of each term on the left hand side and (ii) we recover (67) by assuming the friction term is ~ 0. Let us begin by checking (ii), we can write (90) under these assumptions as

$$\int d\upsilon f' v_f^2 f'' = \int d\upsilon f' \frac{dV}{df}. \tag{91}$$

We deconstruct the integrals such that both are trivial integrations

$$v_f^2 \int \cancel{d\upsilon} \frac{d}{\cancel{d\upsilon}} \left(\frac{f'^2}{2} \right) = \int \cancel{d\upsilon} \frac{\cancel{df}}{\cancel{d\upsilon}} \frac{dV}{\cancel{df}}. \tag{92}$$

We recover our EOM with an extra constant of c,

$$\int dV = V(f) + c = v_f^2 \frac{f'^2}{2}. \tag{93}$$

This constant is 0 to preserve our conditions (47). With this result we can confirm that the left hand side of our (88) is very small. We must confirm condition (i), f'' and $\frac{dV}{df}$ are of a significantly greater order than $\frac{3v_f^2}{\upsilon} f'$. We must only verify that this is true for one of the two terms as we have already shown condition (ii) that the two left hand terms are essentially equal in the TWL. We can show this similarly to the previous condition, by multiplying in a factor of f'. Quickly we see that we can use the EOM to evaluate further,

$$v_f^2 \int_{R-\delta}^{R+\delta} d\upsilon \frac{3}{\upsilon} f' \to v_f^2 \int_{R-\delta}^{R+\delta} d\upsilon \frac{3}{\upsilon} (f'^2) = 3v_f \int_{R-\delta}^{R+\delta} d\upsilon \frac{f'\sqrt{2V}}{\upsilon}. \tag{94}$$

In the last step we have taken into account that we are interested in the wall region and applied our EOM (103). We can take another effect from this TWL and note that the limits of integration are very close together, separated only by the thickness of the wall which we have defined as extremely small. With this we can approximate any factors of υ as constants equal to the radius of the wall, which we write as R. In the same step we decompose the f' factor

$$3v_f \int_{R-\delta}^{R+\delta} d\upsilon \frac{f'\sqrt{2V}}{\upsilon} = \frac{3v_f}{R} \int_0^1 \cancel{d\upsilon} \frac{df}{\cancel{d\upsilon}} \sqrt{2V} = \frac{3v_f}{R} \int_0^1 df \sqrt{2V}. \tag{95}$$

Our last piece can be noted as our definition of the wall tension. We have finally an expression for the friction contribution,

$$v_f \int_{R-\delta}^{R+\delta} d\upsilon \frac{3}{\upsilon} (f'^2) = \frac{3\sigma}{R}. \tag{96}$$

We have computed our σ explicitly as (60) so we may write our friction (96) explicitly with (60),

$$\frac{3}{R}\sigma = \frac{3}{R} \frac{\sqrt{\lambda_6} v_f^4}{8}. \tag{97}$$

We must now show that for the left term from (93), within the wall $V(f) >> \frac{3\sigma}{R}$. The left hand side of this inequality is straightforward, with V_{Max} from (19) marking the potential in the wall region

$$\frac{3\sigma}{R} \frac{1}{V_{Max}} = \frac{1}{R} \frac{81}{4v_f^2} \sim O(1/R). \tag{98}$$

We have that this friction term (96) is of $O(\sigma/R)$. Our final step is to show that R is sufficiently large such that the friction is vanishing within the wall in the action. We see υ as an analog of R in (97) where υ may be smaller than R. We must confirm that

$$\frac{\Delta\upsilon}{\upsilon} \sim \varepsilon. \tag{99}$$

If $\upsilon < R$ and (99) then we confirm the friction term (97) is negligible. When computing $\Delta\upsilon$ we must define limits of f that mark the bounds of the wall. We may choose this conservatively to be $\frac{1}{4} < f < \frac{3}{4}$, giving

$$\Delta\upsilon = \int d\upsilon = \nu_f \int_{\frac{1}{4}}^{\frac{3}{4}} \frac{df}{\sqrt{2V(f)}} = \frac{1}{\nu_f^2\sqrt{\lambda_6/4}} \int_{\frac{1}{4}}^{\frac{3}{4}} df \frac{1}{f(f^2-1)}. \tag{100}$$

We transform following directly from (67) after which we have taken the limit $\varepsilon \to 0$. We find

$$\Delta\upsilon = \frac{1}{\sqrt{\lambda_6}\nu_f^2} log\left(\frac{135}{7}\right) \sim O\left(\frac{1}{\sqrt{\lambda_6}\nu_f^2}\right), \qquad [\Delta\upsilon] = -1. \tag{101}$$

The nature of our problem is such that we are only interested in cases where the bubble is stable and the volume energy surpasses or is equal to the surface energy. We found the minimum radius for which this is true to be υ_0 from (62), we find

$$\frac{\Delta\upsilon}{\upsilon} \leq \frac{\Delta\upsilon}{\upsilon_0} = log\left(\frac{135}{7}\right) \frac{1}{\sqrt{\lambda_6}\nu_f^2} \frac{\sqrt{\lambda_6}\nu_f^2\varepsilon}{3} \sim \varepsilon. \tag{102}$$

With our result and $\upsilon_0 \leq R$, we have confirmed R is sufficiently large such that (97) is of $O(\varepsilon)$. We finally have

$$\nu_f^2 \frac{f'^2}{2} = V(f), \tag{103}$$

which we can safely use in our action computations.

3 Cosmic Strings

In this section we would like to introduce the Cosmic string. We will approach the problem as a classical field configuration and derive the EOM for the global and local cases. We will then discuss the effects such an object has in space, possible methods of detection and produced signals.

Our Cosmic strings are defects produced by U(1) symmetry breaking. Our discussed potential has a solution of the Coleman bubble, the same potential gives way to the static cosmic string. We generally consider some temperature dependent potential, that at high temperatures has a U(1) symmetry. As temperature decreases, the temperature dependence can create a new minimum. The field will find itself in one of the two minima separated by a potential wall. We consider this potential to be at 0 temperature and of the form (16). We can begin describing our cosmic string with a general lagrangian density of the form

$$\mathscr{L} = -\frac{1}{4}F^{\mu\nu}F_{\mu\nu} - D_\mu\phi^* D^\mu\phi - V(|\phi|), \tag{104}$$

where

$$F_{\mu\nu} = \partial_\mu A_\nu - \partial_\nu A_\mu \qquad \text{and} \qquad D_\mu\phi = \partial_\mu\phi - ieA_\mu\phi. \tag{105}$$

We have our vector field A_μ which couples to the scalar field with charge e. The potential we are interested in is described in Section 1.1 where we have a true vacuum surrounded by a false minimum separated by a potential wall of height V_{Max}. The potential we have chosen is shown in Figure 3.1. We will make an ansatz for the field ϕ that reflects this as a phase contribution. Our phase contribution will have no impact on the amplitude of the field. Our ansatz for such a field is

$$\phi_{r,\theta} = \frac{v_f}{\sqrt{2}}e^{in\theta}f(r) \qquad \text{and} \qquad \lim_{r\to\infty}\phi = \frac{v_f}{\sqrt{2}}e^{in\theta}. \tag{106}$$

Where we have chosen the coordinates to be polar in x and y such that

$$r = \sqrt{x^2+y^2}, \quad \theta = arctan\left(\frac{x}{y}\right), \tag{107}$$

giving

$$g^{\mu\nu}(t,x,y,z) = \begin{bmatrix} -1 & 0 & 0 & 0 \\ 0 & 1 & 0 & 0 \\ 0 & 0 & 1 & 0 \\ 0 & 0 & 0 & 1 \end{bmatrix} \rightarrow g^{\mu\nu}(\tau,r,\theta,z) = \begin{bmatrix} 1 & 0 & 0 & 0 \\ 0 & 1 & 0 & 0 \\ 0 & 0 & \frac{1}{r^2} & 0 \\ 0 & 0 & 0 & 1 \end{bmatrix}. \tag{108}$$

We consider the phase θ in our potential. If we trace a circle of centered around the true minimum, we have a phase beginning at $\theta = 0$ increasing until it reaches $\theta = 2\pi$ where it resets and continues. We consider how one might continuously shrink that circle down to a

point at the true minimum. We find this is impossible to do while maintaining a defined phase θ. At our true minimum point we have that the phase is all values in $[0,2\pi]$ simultaneously, and thus undefined. This line of undefined phase θ is the core of our string (lying on the z axis in real space), a one dimensional defect. As a result our phase contribution we see that these cosmic strings can only exist as either infinitely long or loops.

Let us now discuss the U(1) vector field A_μ. We make an ansatz for our gauge field A_μ as in [29], describing how the field looks and changes throughout space, notably independent of position in the z and τ directions. This is written as

$$A_i = -\frac{n\varepsilon_{ij}x^j}{er^2}a(r), \quad i:(x,y), \tag{109}$$

where we have the levi-cevita symbol ε, which is antisymmetric with $\varepsilon^{12} = \varepsilon_{12} = 1$

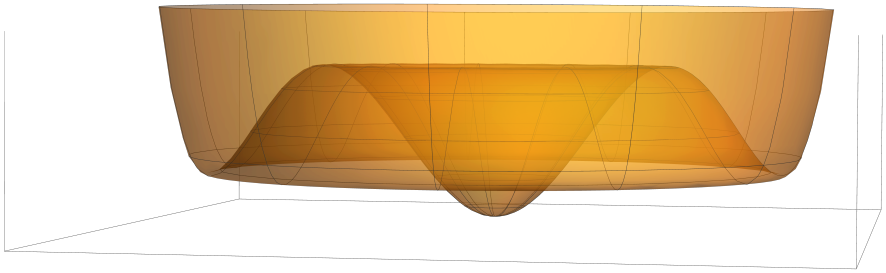

Figure 3.1. A three dimensional rendering of our wine bottle potential.

We would like to convert $A_{x,y,\rho}$ into our polar coordinates for simplicity. The basis vectors of the plane perpendicular to the string are

$$\hat{e}_x = (1,0) \qquad \text{and} \qquad \hat{e}_y = (0,1). \tag{110}$$

We write our new basis vectors in terms of r and θ with r denoting the radial distance from the string and θ the angle between the x and y components

$$\hat{e}_r = (cos\theta, sin\theta), \qquad \hat{e}_\theta = (-sin\theta, cos\theta). \tag{111}$$

We then write our A_r and A_θ with the above identities

$$A_r = A_x cos\theta + A_y sin\theta = -\frac{nxy}{er^2}a(r) + \frac{nxy}{er^2}a(r) = 0, \tag{112}$$

$$A_\theta = -A_x sin\theta + A_y cos\theta = \frac{nx^2}{er^2}a(r) + \frac{ny^2}{er^2}a(r) = \frac{n}{e}a(r). \tag{113}$$

Our lagrangian becomes significantly simpler immediately as only A_θ is non-zero and all other gauge field terms vanish. Referring to our definition (105), we can write some of the terms as now μ, ν sum over r, θ, z, τ:

$$F_{rr} = F_{\theta\theta} = F_{zz} = F_{zr} = F_{z\tau} = F_{\tau r} = F_{\tau\tau} = 0. \tag{114}$$

The only non-zero component being

$$F_{\theta r} = -F_{r\theta} = (\cancelto{0}{\partial_\theta A_r} - \partial_r A_\theta) = -\frac{n}{e}\partial_r a. \tag{115}$$

We can follow the same procedure for the covariant derivative terms in (105) to find

$$D_\theta = \partial_\theta - ie\frac{n}{e}a(r) = \partial_\theta - ina, \tag{116}$$

such that

$$D_\theta\phi = \partial_\theta\phi - ie\frac{n}{e}a(r)\phi = in\phi - ina(r)\phi = in\phi(1-a(r)). \tag{117}$$

which gives an important result for outside the wall, where $f = 1$ and $a = 1$ we find $D_\mu\phi = 0$. We can write our action as

$$\begin{aligned} S_E = 2\pi\int drd\tau dzr\Big[-\frac{1}{4}[2g^{\theta\theta}g^{rr}F_{\theta r}F_{\theta r}] - \\ g^{rr}\partial_r\phi^*\partial_r\phi - g^{\theta\theta}\partial_\theta\phi^*\partial_\theta\phi \\ - ieg^{\theta\theta}A_\theta\phi^*\partial_\theta\phi + ieg^{\theta\theta}A_\theta\phi\partial_\theta\phi^* - g^{\theta\theta}e^2A_\theta A_\theta\phi^*\phi - V(|\phi|)\Big]. \end{aligned} \tag{118}$$

We input all of our elements from $g^{\mu\nu}$ in (108)

$$\begin{aligned} = 2\pi\int drd\tau dzr\Big[-\frac{1}{4}[2\left(\frac{1}{r^2}\right)F_{\theta r}^2] \\ - \partial_r\phi^*\partial_r\phi - \left(\frac{1}{r^2}\right)\partial_\theta\phi^*\partial_\theta\phi \\ - ie\left(\frac{1}{r^2}\right)A_\theta\phi^*\partial_\theta\phi + ie\left(\frac{1}{r^2}\right)A_\theta\phi\partial_\theta\phi^* + \left(\frac{1}{r^2}\right)e^2A_\theta A_\theta\phi^*\phi - V(|\phi|)\Big]. \end{aligned} \tag{119}$$

We then fill in all of our field strength tensor components

$$\begin{aligned} = 2\pi\int drd\tau dzr\Big[-\frac{1}{4}[2\left(\frac{1}{r^2}\right)\left(-\frac{n}{e}\partial_r a\right)^2] \\ - \partial_r\phi^*\partial_r\phi - \left(\frac{1}{r^2}\right)\partial_\theta\phi^*\partial_\theta\phi \\ - ie\left(\frac{1}{r^2}\right)(\frac{n}{e}a)\phi^*\partial_\theta\phi + ie\left(\frac{1}{r^2}\right)(\frac{n}{e}a)\phi\partial_\theta\phi^* + \left(\frac{1}{r^2}\right)e^2(\frac{n}{e}a)^2\phi^*\phi - V(|\phi|)\Big]. \end{aligned} \tag{120}$$

We can continue by including the ansatz for the field ϕ

$$\partial_r\phi = \frac{v_f}{\sqrt{2}}e^{in\theta}\partial_r f \qquad \text{and} \qquad \partial_\theta\phi = in\frac{v_f}{\sqrt{2}}e^{in\theta}f, \tag{121}$$

such that our lagrangian is

$$
\begin{aligned}
&= 2\pi \int drd\tau dzr\Big[-\frac{1}{4}[2\Big(\frac{1}{r^2}\Big)\Big(-\frac{n}{e}\partial_r a\Big)^2] \\
&\quad -\partial_r\Big(\frac{v_f}{\sqrt{2}}e^{-in\theta}f\Big)\partial_r\Big(\frac{v_f}{\sqrt{2}}e^{in\theta}f\Big) - \Big(\frac{1}{r^2}\Big)\partial_\theta\Big(\frac{v_f}{\sqrt{2}}e^{-in\theta}f\Big)\partial_\theta\Big(\frac{v_f}{\sqrt{2}}e^{in\theta}f\Big) \\
&\quad -ie\Big(\frac{1}{r^2}\Big)\Big(\frac{n}{e}a\Big)\Big(\frac{v_f}{\sqrt{2}}e^{-in\theta}f\Big)\partial_\theta\Big(\frac{v_f}{\sqrt{2}}e^{in\theta}f\Big) \\
&\quad +ie\Big(\frac{1}{r^2}\Big)\Big(\frac{n}{e}a\Big)\Big(\frac{v_f}{\sqrt{2}}e^{in\theta}f\Big)\partial_\theta\Big(\frac{v_f}{\sqrt{2}}e^{-in\theta}f\Big) \\
&\quad +\Big(\frac{1}{r^2}\Big)e^2\Big(\frac{n}{e}a\Big)^2\Big(\frac{v_f}{\sqrt{2}}e^{-in\theta}f\Big)\Big(\frac{v_f}{\sqrt{2}}e^{in\theta}f\Big) - V(|\phi|)\Big]. \quad (122)
\end{aligned}
$$

All of the phase θ exponential factors cancel and our action simplifies to

$$
\begin{aligned}
&= 2\pi \int drd\tau dzr\Big[-\frac{1}{4}[\Big(\frac{2n^2}{e^2r^2}\Big)(\partial_r a)^2] \\
&\quad -\frac{v_f^2}{2}(\partial_r f)^2 - \frac{v_f^2 n^2 f^2}{2r^2} + \frac{n^2 v_f^2 f^2}{2r^2}a + \frac{n^2 v_f^2 f^2}{2r^2}a \\
&\quad +\left(\frac{n^2 v_f^2}{2r^2}\right) f^2 a^2 - V(|\phi|)\Big], \quad (123)
\end{aligned}
$$

we can combine all the terms with a factor of $\left(\frac{n^2 v_f^2}{2r^2}\right) f^2$

$$
\begin{aligned}
&= 2\pi \int drd\tau dzr\Big[-\frac{1}{4}[\left(\frac{2n^2}{e^2r^2}\right)(\partial_r a)^2] \\
&\quad -\frac{v_f^2}{2}(\partial_r f)^2 - \frac{v_f^2 n^2 f^2}{2r^2}(1-a)^2 - V(|\phi|)\Big]. \quad (124)
\end{aligned}
$$

Our lagrangian density in our chosen polar coordinates is then

$$
\mathscr{L} = r\Big[-\left(\frac{n^2}{2e^2r^2}\right)(\partial_r a)^2 - \frac{v_f^2}{2}(\partial_r f)^2 - \frac{v_f^2 n^2 f^2}{2r^2}(1-a)^2 - V(|\phi|)\Big]. \quad (125)
$$

We would like to now compute the EOM for the scalar field f and the gauge field a

$$
\frac{d}{dr}\frac{\partial \mathscr{L}}{\partial(\partial_r f)} - \frac{\partial \mathscr{L}}{\partial f} = 0 \qquad \text{and} \qquad \frac{d}{dr}\frac{\partial \mathscr{L}}{\partial(\partial_r a)} - \frac{\partial \mathscr{L}}{\partial a} = 0. \quad (126)
$$

When evaluated these are:

$$
\boxed{\partial_r^2 a - \frac{1}{r}\partial_r a + 2v_f^2 f^2 e^2 (1-a) = 0} \quad (127)
$$

$$\boxed{\partial_r^2 f + \frac{\partial_r f}{r} - \frac{n^2 f}{r^2}(1-a)^2 - \frac{1}{v_f^2}\frac{dV}{df} = 0} \tag{128}$$

Let us for a moment consider the region outside the string. For our gauge field a, in order to satisfy the EOM, we must require that at some distance r the field becomes constant, at that we need the constant to be 1. Let us now consider the second EOM. We have previously chosen an ansatz for f such that outside the string f is constant. We must finally consider the case inside of the string. Following our choice of the TWL, our field f is 0 and constant, this solves our EOM for f. Our a is slightly more complex but we see that as in [29], $a(r) = \frac{r^2}{R^2}$ solves our equation. With this we have the bounds

$$0 \leq r < R \qquad \begin{cases} f(r) = 0 \\ a(r) = \frac{r^2}{R^2} \end{cases} \qquad \text{and} \qquad R \leq r \qquad \begin{cases} f(r) = 1 \\ a(r) = 1 \end{cases} \tag{129}$$

where R refers to the radius of the string.

3.1 Global VS Local String

In this section we will work out some differences between local and global cosmic strings. Let us consider the general lagrangian (33), specifically the kinetic term. We are interested in how this term behaves in the limit of $r \to \infty$ as the rest of the terms are well behaved. In our later computations we focus on the global symmetry case but before we make this specification, we discuss the difference between the two classifications.

3.1.1 Local Symmetry

Beginning by discussing the local case (also called gauge symmetric case) where the scalar field and gauge field are invariant under a local transformation. The choice of the gauge field A_μ follows from the specification that the kinetic term vanishes outside of the string wall. Using the definition of the covariant derivative D_μ in (34), we find that this is accomplished if

$$A_\mu \sim \frac{1}{ie}\partial_\mu(\ln\phi) = \frac{1}{ie}\frac{1}{\phi}\partial_\mu\phi. \tag{130}$$

We previously computed $D_\mu\phi$ in (117). Looking outside the string wall, we have $a(r) = 1$ from (129), this results in the kinetic term vanishing outside of the string as desired. We need not worry about this term diverging within the string as it is bounded by the radius. Next we would like to investigate the local gauge transformation

$$\phi \to \tilde{\phi}e^{i\alpha(x)} \qquad \text{and} \qquad A_\mu \to \tilde{A}_\mu + \frac{1}{e}\partial_\mu\alpha(x), \tag{131}$$

where here the argument "x" is an arbitrary point in space. We confirm that our terms in (33)

are invariant under such a transformation, writing

$$D_\mu\phi \to \partial_\mu\tilde{\phi}e^{i\alpha(x)} - ie\left(\tilde{A}_\mu + \frac{1}{e}\partial_\mu\alpha(x)\right)\tilde{\phi}e^{i\alpha(x)}$$
$$= \left(\partial_\mu\tilde{\phi} - ie\tilde{A}_\mu\right)e^{i\alpha(x)} + i\partial_\mu\alpha(x)\tilde{\phi}e^{i\alpha(x)} - i\partial_\mu\alpha(x)\tilde{\phi}e^{i\alpha(x)}$$
$$= \tilde{D}_\mu\tilde{\phi}e^{i\alpha(x)}. \quad (132)$$

We can easily then see the invariance of the kinetic term, i.e. $\tilde{D}_\mu\tilde{\phi}^*\tilde{D}^\mu\tilde{\phi} = D_\mu\phi^* D^\mu\phi$. Our potential term $V(|\phi|)$ transforms trivially as $|\tilde{\phi}| = |\phi|$. Finally, we must consider $F^{\mu\nu}F_{\mu\nu}$ and show its invariance. From

$$\partial_\mu A_\nu - \partial_\nu A_\mu \to (\partial_\mu\tilde{A}_\nu - \partial_\nu\tilde{A}_\mu) + \frac{1}{e}\partial_\nu\partial_\mu\alpha(x) - \frac{1}{e}\partial_\mu\partial_\nu\alpha(x) = \partial_\mu\tilde{A}_\nu - \partial_\nu\tilde{A}_\mu, \quad (133)$$

we conclude that

$$F^{\mu\nu}F_{\mu\nu} = \tilde{F}^{\mu\nu}\tilde{F}_{\mu\nu}. \quad (134)$$

With our condition that at large r our field function $a(r) \to 1$ we see that the field strength tensor in (105) and our covariant derivative both vanish outside the string. We defined the potential such that outside of the string the vacuum energy density is vanishing. Our action for such a configuration is then convergent as desired, and we can safely integrate over all space. Let us now consider what this gauge field means physically. The local string has some enclosed magnetic flux within the core of the string shown with Stokes theorem

$$\Phi_B = \int B\cdot dS = \oint A\cdot dl = \int d\theta\frac{1}{ie}\frac{1}{\phi}\partial_\theta\phi = \frac{2\pi n}{e}. \quad (135)$$

We have taken definitions for A_μ from (130) to show that the magnetic flux is proportional to the winding number n and charge e. So long as $n > 0$ we have some magnetic flux through the core of the string. Crucially, this magnetic flux is quantized in units of $\frac{2\pi}{e}$ as $n \in \mathbb{N}$.

3.1.2 Global Symmetry

We move to the global string case and consider our action and lagrangian density again. In the local case our transformation (131) had a spatially dependent phase $\alpha(x)$. For the global case this phase becomes a constant

$$\alpha(x) \to const, \quad (136)$$

and we can set the gauge field A_μ to be 0 consistently. Our potential term $V(|\phi|)$ transforms just the same as in the local case. Finally, the kinetic term causes some issues in the evaluation of the action. We find ourselves with a term of the form

$$\int d\rho dr\rho r(\partial_\mu\phi^*\partial^\mu\phi) \supset \int d\rho\rho\left(n^2\ln\left(\frac{R_{Max}}{R}\right)\right), \quad (137)$$

where we used that $\phi \propto e^{in\theta}$. We have had to impose an upper bound on the radius R_{Max}. Without such a bound the term is divergent and thus so is the bounce action. Physically, R_{Max} can be interpreted as the average separation between strings in a network of cosmic strings. Designating a maximal radius allows us to actually interpret results later when computing the

action. This bound is only necessary when computing the action of the static string. When we compute the properly normalized bounce action this R_{Max} dependence disappears and we need not assign it a specific value. This global symmetry case proves to be significantly more simple to evaluate analytically (up until the ρ integration) and thus we will continue with the global choice.

3.2 Spatial Geometry of a Cosmic String

3.2.1 String Tension

In literature concerning cosmic strings estimated to be extremely thin, the string is often entirely defined by its tension μ, the energy per unit length. In contrast in this thesis strings are described as cylindrical objects with a (thin) wall at the radial position $R(z) = r$. In other words, our discussion assumes a non-vanishing string width, thus before we continue with external geometry of a cosmic string we must draw a connection between our wall tension σ and the string tension μ. We only consider μ for the *local* cosmic string as the energy is divergent at large distances from the wall in the global case, this divergence is discussed in the previous section. The energy of the local cosmic string in our TWL is computed in [31] as

$$\mu = \frac{E(R)}{L} = \underbrace{-\pi R^2 \Delta V + \frac{2\pi n^2}{e^2 R^2}}_{interior} + \underbrace{2\pi R\sigma}_{wall}. \tag{138}$$

3.2.2 The Deficit Angle

When we analyze the gravitational field around a straight cosmic string we discover some very interesting effects, namely the deficit angle, computed in [32, 39–41]. Here we provide a brief review of its derivation. The energy momentum tensor is $T^{\nu}_{\mu} = \mu \times diag(1,0,0,1)$ (in cartesian coordinates) along the length of the string, outside it is vanishing. To find the angle deficit we take the weak field limit meaning we estimate the metric to be nearly Minkowski and write

$$g^{\mu\nu} = \eta^{\mu\nu} + h^{\mu\nu}. \tag{139}$$

where $h^{\mu\nu} << 1$. One then solves the Einstein equations

$$(\Delta^2 - \partial_t^2) h_{\mu\nu} = 16\pi G(T_{\mu\nu} - \frac{1}{2}\eta_{\mu\nu}T), \tag{140}$$

under the Lorentz gauge

$$\partial_\mu (h^{\mu}_{\nu} - \frac{1}{2}\delta^{\mu}_{\nu} h) = 0, \tag{141}$$

often a convenient choice when considering GW. The solutions to (140) for a vacuum string give us the gravitational field

$$h_{00} = h_{33} = 0$$

and

$$h_{11} = h_{22} = 8\mu G \ln\left(\frac{r}{R}\right)$$

where R is the string radius and $r = \sqrt{x^2 + y^2}$ is the distance from the center of symmetry. We can immediately see an interesting effect, as we travel further from the string the gravitational field strength grows. The attached string tension factor μ lets us continue by writing out the metric in cylindrical coordinates

$$ds^2 = dt^2 - dz^2 - \left(1 - 8\pi\mu G \ln\left(\frac{r}{R}\right)\right)(dr^2 + r^2 d\phi^2), \tag{142}$$

then performing a coordinate transformation $r' = \sqrt{\ln\left(\frac{r}{R}\right)}r$ we have a metric of the form

$$ds^2 = dt^2 - dz^2 - dr'^2 - (1 - 8\pi\mu G)\, r'^2 d\phi^2. \tag{143}$$

We can clearly see an angle deficit of $8\pi G\mu$. This results in a conical warping of space-time with the point of the cone lying at the center of the string. At this moment we would like to make several comments: (i) the deficit angle δ is suppressed by the Planck mass and thus a tiny effect; explicitly $\delta = 8\pi\mu G = \frac{\mu}{M_{Pl}^2} << 1$ for sub-Planckian string tensions, where we used the definition of the reduced Planck mass ${M_{Pl}}^2 = \frac{1}{8\pi\mu G}$.

(ii) The same formula for δ holds approximately for a local cosmic string with finite thickness far away from the string core.

(iii) For calculating the bounce action, which is the purpose of this work, we can safely neglect the gravitational back-reaction of the string if we are in the typical regime where $\mu << M_{Pl}^2$ and thus $\delta << 1$. This is also in line with the standard Coleman calculation of the $O(4)$ bounce action, which also neglects gravitational back reaction (also here including gravity required a generalized treatment [42]).

(iv) In the case when $\delta = O(1)$ a more complicated solution beyond the scope of this work would be needed where the ansatz T_μ^ν reflects the $O(2) \times O(2)$ symmetry of the bounce configuration. We stress however that this would require Planck scale string tensions. Instead, in realistic production scenarios typically $\mu << M_{Pl}^2$.

3.2.3 Observable Effects of Simple Cosmic Strings

We generally consider the limit of an infinitely thin string while discussing any observable effects. The effects that such an object could produce are incredibly unique as the $O(2)$ symmetry of the string is a stark juxtaposition with the homogeneity and isotropy of the setting.

Gravitational lensing refers to the deflection of photons by gravitational fields, a phenomenon that can be seen around massive objects such as black holes. In such cases the image will have a curved shape appearing as a halo around the horizon of the object between the observer and the source [43]. In the case of the cosmic string the lensing would result in a double image on either side of the string [11, 40], no other theorized object could produce such an effect, making it all the more exciting.

Another possible effect would be found in observation of the CMB. If we consider the strings at very early times, moving very fast-we find that the surrounding matter will experience a boost into the wake of the string [12, 44]. In the wake particles from either direction perpendicular to the velocity of the string and the length will collide and heat up, resulting in

a polarization. In the CMB this would show up as polarized rectangles, just as in the case of gravitational lensing, no other object could create such an effect.

In recent years astrophysicists have been observing Large Scale Structures that surpass homogeneity scales [45]. These objects are the Giant Arc [46] and the Big Ring [47]. Cosmic strings are interesting for such conversations as the straight strings are of an infinite length and thus can extend beyond the homogeneity scale.

It is clear that Cosmic Strings could have diverse and interesting effects both through a theoretical and astrophysical lens. While the observational effects are obviously exciting, we will continue our discussion in a theoretical capacity.

4 String Induced Tunneling

The Coleman bubble is at this point a well understood mechanism for vacuum decay, we expand this method to the case of the O(2)×O(2) symmetric configuration. Our generalization takes the cosmic string defect as a starting point, where we define an infinite line (in our case along the z axis) marking the core of the string. Our configuration is such that the field in the core of the string sits in the true vacuum, outside of the string core the field sits in the metastable vacuum as described in Figure 1.2. The two minima of our potential are separated by a potential barrier and the field in the wall region interpolates between these two minima, illustrated in Figure 2.2. Our cosmic string differs from the usually discussed stable cosmic string as in such cases the core of the string sits at a potential maximum where in all directions there lies a true minimum. In our case the linear vacuum defect is a straight line even though a cosmic string need not be straight, we have simply chosen to analyze a very small section of the string such that it can be treated as straight.

Our analysis follows Coleman's methods [1] and, as opposed to prior work in [29], will include relativistic corrections. We focus on the global string case for simplicity. For this choice there is no gauge field, which we reflect in our computation by setting $A_\mu = 0$. We have discussed the spherical $O(3) \times \tau$ case where there is no notion of a winding number. We can understand this by imagining a connected path along the surface of the sphere. We can smoothly shrink this path to a point without any discontinuities or undefined values in the field ϕ. In particular, we can take the field to be real everywhere. Now, our symmetry is broken into $O(2) \times O(2)$ and our configuration requires winding to be included in our bounce action. This is done by including a non-trivial complex phase $n\theta$, where n is the winding number. In contrast to the spherical case, a loop around the string cannot be collapsed into a point smoothly as along the z axis the phase becomes undefined, occupying all values in the interval $[0, 2\pi]$ at once. We focus on the leading order of the tunneling amplitude and will provide an order of magnitude estimate for the prefactor. We consider a section of the string tunneling to critical radius that we call R_c just as in the spherical case. Our global action is then written as

$$S_E^{2\times 2} = \int dx^4 [-\partial_\mu \phi^* \partial^\mu \phi - V(|\phi|)]. \tag{144}$$

To reflect our string setup symmetries we adjust the symmetries of our computation. Our new radial coordinates are

$$\rho^2 = \tau^2 + z^2 \qquad \text{and} \qquad r^2 = x^2 + y^2, \tag{145}$$

each of them corresponding to one $O(2)$ factor. Our field ϕ is parametrized as

$$\phi(r, \rho, \theta) = \frac{v_f}{\sqrt{2}} f(r, \rho) e^{in\theta}, \tag{146}$$

such that we have our winding number n, angular coordinate θ, distance from the axis of symmetry r, with f being our real scalar field function. We can use our parametrization to recover our potential (46). Our action is then written in terms of this new parametrization as

$$S_E^{2\times 2} = \int dx^4 \left[\frac{v_f^2}{2} [\partial^\mu (f e^{-in\theta}) \partial_\mu (f e^{in\theta})] + \frac{\lambda_6 v_f^6}{8} (f^2 - \varepsilon)(f^2 - 1)^2 \right]. \tag{147}$$

We have not yet converted our differential elements to $d\rho$ and dr yet, the index μ now covers ρ, r and θ. We re-parametrize by performing two polar coordinate transforms

$$\rho = \sqrt{\tau^2 + z^2}, \quad \theta_1 = \arctan\left(\frac{\tau}{z}\right)$$

and

$$r = \sqrt{x^2 + y^2}, \quad \theta = \arctan\left(\frac{x}{y}\right). \tag{148}$$

The determinant of the jacobian informs our re-parametrization in the action with

$$det^{-1} \begin{bmatrix} \frac{\partial\rho}{\partial x} & \frac{\partial\rho}{\partial y} & \frac{\partial\rho}{\partial z} & \frac{\partial\rho}{\partial\tau} \\ \frac{\partial\theta_1}{\partial x} & \frac{\partial\theta_1}{\partial y} & \frac{\partial\theta_1}{\partial z} & \frac{\partial\theta_1}{\partial\tau} \\ \frac{\partial r}{\partial x} & \frac{\partial r}{\partial y} & \frac{\partial r}{\partial z} & \frac{\partial r}{\partial\tau} \\ \frac{\partial\theta}{\partial x} & \frac{\partial\theta}{\partial y} & \frac{\partial\theta}{\partial z} & \frac{\partial\theta}{\partial\tau} \end{bmatrix} = det^{-1} \begin{bmatrix} 0 & 0 & \frac{z}{\rho} & \frac{\tau}{\rho} \\ 0 & 0 & -\frac{\tau}{\rho^2} & \frac{z}{\rho^2} \\ \frac{x}{r} & \frac{y}{r} & 0 & 0 \\ \frac{y}{r^2} & -\frac{x}{r^2} & 0 & 0 \end{bmatrix} = \rho r. \tag{149}$$

The θ and θ_1 integrations give a factor of 2π each and we have an action

$$S_E^{2\times 2} = 4\pi^2 \int dr d\rho \rho r \left[\frac{v_f^2}{2} \left[\left(\frac{\partial f}{\partial \rho}\right)^2 + \left(\frac{\partial f}{\partial r}\right)^2 + \frac{n^2 f^2}{r^2} \right] + V(f) \right]. \tag{150}$$

While the action appears to be much more simple, there is an observation we can make to simplify our computations. Our field function f can be assigned some limits. In the core of the string where $r = 0$ we are close to the true minimum: $f \simeq 0$ and our potential is $-\Delta V$ from (17). Outside the wall, we are in a false vacuum and $f = 1$. We define $\frac{df}{d\zeta} = f'$ and at this point like to make an observation for f' in our scenario. We have $f' = 0$ inside and outside of the string, while it can take on finite values within the wall region. This behavior is a result of our use of the TWL. We will later consider how the $O(2) \times O(2)$ symmetry affects this regime. In summary we impose two boundary conditions

$$f'(r \to 0, \rho) = 0 \qquad \text{and} \qquad f(r \to \infty, \rho) = 1, \tag{151}$$

which are enough to close the system. This set of limits paired with the symmetry of the field profile and dynamical equations arising from (150) are referred to as the bounce solution, which was studied for this symmetry in [30]. We would like to make one further ansatz for our field function f reflecting how the function actually behaves in the TWL, just as we did in the O(3) symmetric Bubble discussion in Section 2.4. We have repeatedly defined the field function to be a constant inside and outside of the bubble. One can identify that f is a function of proximity to the wall at radial position $r = R(\rho)$. We combine this behaviour

and the assumption that the wall will expand at relativistic speeds to define a new function ζ, defined as

$$\zeta = \gamma(r-R), \tag{152}$$

that reflects this behaviour of

$$f(\rho,r) = f_{wall}(\zeta) = f_{wall}(\gamma(\rho)(r-R(\rho)), \tag{153}$$

where we have defined the Lorentz factor $\gamma(\rho)$ to reflect the Lorentz contraction of the thickness of the wall as it moves with relativistic speeds. For convenience we will henceforth drop the "wall" subscript. We also stress that the ansatz in (153) differs from that in [30] where the ansatz is in the non-relativistic limit where $\gamma \simeq 1$,

$$\gamma(\rho) = \frac{1}{\sqrt{1+\left(\frac{\partial R(\rho)}{\partial \rho}\right)^2}}. \tag{154}$$

In (154) we have a "+" sign where typically there would be a "-" as an artifact of our Euclidian time choice. With our new parametrization we can write our action yet again in a new form

$$S_E^{2\times 2} = 4\pi^2 \int d\rho dr r\rho \left[\frac{v_f^2}{2}\left(\frac{\partial f}{\partial \zeta}\right)^2\left[\left(\frac{\partial \zeta}{\partial \rho}\right)^2+\left(\frac{\partial \zeta}{\partial r}\right)^2\right]+\frac{v_f^2 n^2 f^2}{2r^2}+V(f)\right]. \tag{155}$$

It is useful to know the EOM found from this action

$$\frac{d}{d\zeta}\frac{\partial \mathscr{L}}{\partial(\partial_\zeta f)}-\frac{\partial \mathscr{L}}{\partial f}=0, \tag{156}$$

where the lagrangian density is

$$\mathscr{L} = r\rho\left[\frac{v_f^2}{2}\left(\frac{\partial f}{\partial \zeta}\right)^2\left[\left(\frac{\partial \zeta}{\partial \rho}\right)^2+\left(\frac{\partial \zeta}{\partial r}\right)^2\right]+\frac{v_f^2 n^2 f^2}{2r^2}+V(f)\right]. \tag{157}$$

We can write the multiplicative term as $r = \frac{\zeta}{\gamma}+R$ and treat ρ as a constant in this evaluation as ζ does not explicitly have any dependence on ρ. Evaluating different terms in (156), we obtain

- $\frac{\partial \mathscr{L}}{\partial(\partial_\zeta f)} = v_f^2 \rho r \partial_\zeta f[(\partial_\rho \zeta)^2+(\partial_r \zeta)^2]$,
- $\frac{\partial}{\partial \zeta}\frac{\partial \mathscr{L}}{\partial(\partial_\zeta f)} = v_f^2 \rho r\left[\partial_\zeta^2 f[(\partial_\rho \zeta)^2+(\partial_r \zeta)^2]+\partial_\zeta f \partial_\zeta[(\partial_\rho \zeta)^2+(\partial_r \zeta)^2]\right]$
  $+ v_f^2 \frac{\rho}{\gamma}\partial_\zeta f[(\partial_\rho \zeta)^2+(\partial_r \zeta)^2]$,
- $\frac{\partial \mathscr{L}}{\partial f} = \rho r(\frac{v_f^2 n^2 f}{r^2}+\frac{dV}{df})$,

we therefore find an EOM

$$\frac{n^2 f}{r}+\frac{r}{v_f^2}\frac{dV}{df}-rf''[(\partial_\rho \zeta)^2+(\partial_r \zeta)^2]$$
$$-f'(r\partial_\zeta[(\partial_\rho \zeta)^2+(\partial_r \zeta)^2]+\gamma^{-1}[(\partial_\rho \zeta)^2+(\partial_r \zeta)^2])=0. \tag{158}$$

This looks somewhat overwhelming. In the following section we will consider it in the TWL which will simplify the problem considerably.

4.1 Thin Wall Limit for Cosmic Strings

By assuming the energy difference between the true and false vacuum "ε", is very small, and the height of the potential barrier V_{Max} in Figure 1.2 is very large, we can make some simplifications. We will only be using the EOM in the wall region, while computing the action. With this we can proceed to find an EOM specifically for the wall region as we did in the spherical cases from the previous section.

Within the wall we have that $R-r=0$ which follows from defining the bubble to be in the TWL. We also define $\dot{R}=\frac{dR}{d\rho}$ and $\dot{\gamma}=\frac{d\gamma}{d\rho}$. Using ζ defined in (152), we derive

$$\partial_\rho \zeta = \dot{\gamma}(r-R)-\dot{R}\gamma = \frac{\dot{\gamma}}{\gamma}\zeta - \dot{R}\gamma \underset{TWL}{\to} -\dot{R}\gamma, \qquad \partial_r \zeta = \gamma, \tag{159}$$

$$\partial_\rho^2 \zeta = \ddot{\gamma}(r-R)-\ddot{R}\gamma-2\dot{R}\dot{\gamma} \underset{TWL}{\to} -\ddot{R}\gamma-2\dot{R}\dot{\gamma}, \qquad \partial_r^2 \zeta = 0. \tag{160}$$

We find

$$(\partial_\rho \zeta)^2+(\partial_r \zeta)^2 = \frac{\dot{\gamma}^2}{\gamma^2}\zeta^2 - 2\dot{\gamma}\dot{R}\zeta + \dot{R}^2\gamma^2+\gamma^2 = \frac{\dot{\gamma}^2}{\gamma^2}\zeta^2 - 2\dot{\gamma}\dot{R}\zeta + 1, \tag{161}$$

replacing some terms with ζ when possible. In the last step of we use our definition of γ in (154). We can compute our $\dot{\gamma}$

$$\frac{d\gamma}{d\rho} = -\frac{1}{2}\frac{2\dot{R}\ddot{R}}{(1+\dot{R}^2)^{3/2}} = -\gamma^3\dot{R}\ddot{R}. \tag{162}$$

We find

$$\partial_\zeta((\partial_\rho \zeta)^2+(\partial_r \zeta)^2) = \partial_\zeta\left(\frac{\dot{\gamma}^2}{\gamma^2}\zeta^2 - 2\dot{\gamma}\dot{R}\zeta + 1\right) = 2\frac{\dot{\gamma}^2}{\gamma^2}\zeta - 2\dot{\gamma}\dot{R} \underset{TWL}{\to} 2\dot{R}^2\ddot{R}\gamma^3, \tag{163}$$

where we set the first term to 0 as $\zeta \sim 0$ when $R \sim r$ and replace the second term with (162). Our new EOM appears,

$$\frac{n^2 f}{R^2} + \frac{1}{v_f^2}\frac{dV}{df} - f'' - f'(2\gamma^3\ddot{R}\dot{R}^2 + R^{-1}\gamma^{-1}) = 0. \tag{164}$$

At this point we find the more nuanced effects of the TWL are useful in simplifying our equation. We would like to show that (164) simplifies such that only the second and third terms remain. We have chosen our bubble radius to be $R(\rho)$. The nature of our problem is such that we are interested in the radius of the $O(2)\times O(2)$ configuration after nucleation (before it starts expanding). We denote the radius at the thickest part of the bulge with R_c. This can then be used as a bound for our bubble wall profile $R(\rho)$

$$R_s < R(\rho) < R_c, \tag{165}$$

where R_s is the static string radius which we will later define explicitly. In our equation there appear some $\dot{R}$ and $\ddot{R}$ terms. We now consider their order of magnitude by defining them.

Since we have identified that the maximal radius of the profile is R_c, we know that any change in the radius of the profile can be at most R_c. Similarly our argument ρ is the coordinate dependent on τ and z. If the bounce had a spherical shape we would have $R(\rho) = \sqrt{R_c^2 - \rho^2}$ which gives $\Delta R \sim R_c$ and $\Delta\rho \sim R_c$. However as our bounce is elongates in the z and τ directions we have $R_c \lesssim \Delta\rho$ and $\Delta R \lesssim R_c$ in general. As a result

$$\frac{dR(\rho)}{d\rho} \sim \frac{\Delta R}{\Delta\rho} \leq \frac{R_c}{R_c} \sim 1. \tag{166}$$

Our estimation is reasonable as we expect the bubble to expand relativistically. To find our $\ddot{R}$ we use the same logic as for $\dot{R}$ and find

$$\frac{d^2R}{d\rho^2} \sim \frac{\Delta\dot{R}}{\Delta\rho} \lesssim \frac{1}{R_c} \lesssim \frac{1}{R}. \tag{167}$$

We can use our estimate for $\dot{R}$ to find γ

$$\gamma = (1+\dot{R}^2)^{-1/2} \lesssim (1+1^2)^{-1/2} \sim 1. \tag{168}$$

We must finally consider the f and f' terms. We have already set our values of f for inside and outside of the bubble in (151) giving $0 \leq f \leq 1$. With respect to the profile of f' and f'', we are interested in their most extreme values, which lie in the wall region along the radial axis (as in Figure 2.2). Our definition in (152) allows us to take $\Delta\zeta \sim \Delta r$ where $\Delta r = |r-R| << R$ giving

$$\frac{df}{d\zeta} = \frac{\Delta f}{\Delta\zeta} = \frac{\Delta f}{\Delta r} \sim \frac{1}{\Delta r} \quad \text{and} \quad \frac{d^2f}{d\zeta^2} = \frac{\Delta f}{\Delta r^2} \sim \frac{1}{\Delta r^2}. \tag{169}$$

Investigating (164) we multiply it by a factor of Δr^2 to make each term dimensionless. We then identify suppressed terms by their order in the wall thinness parameter $\frac{\Delta r}{R}$. Writing our equation as

$$\underbrace{\frac{\Delta r^2 n^2 f}{R^2}}_{a} + \underbrace{\frac{\Delta r^2}{v_f^2}\frac{dV}{df}}_{b} - \underbrace{\Delta r^2 f''}_{c} - \underbrace{\Delta r^2 \underbrace{f'}_{d.1}(2\underbrace{\gamma^3}_{d.2}\underbrace{\ddot{R}}_{d.3}\underbrace{\dot{R}^2}_{d.4} + \underbrace{R^{-1}\gamma^{-1}}_{d.5})}_{d} = 0, \tag{170}$$

we can begin. It is straightforward to check that each term is dimensionless. We can see trivially that term a is of order $O\left((\frac{\Delta r}{R})^2\right)$. Four our term b we can take an estimation from (101) where we explicitly computed the wall thickness and found it to be proportional to the potential difference to the two vacuums, that is to say $\Delta V \sim \frac{v_f^2}{\Delta r^2}$, this results with term b being $O(1)$. Term c follows simply from (169) giving again $O(1)$. From (169), (168), (167), (166) and (168) we have $d.1 - d.5$ respectively. Combined term d has $O(\frac{\Delta r}{R})$. Finally we have each terms order of magnitude

$$\underbrace{\frac{\Delta r^2 n^2 f}{R^2}}_{O((\frac{\Delta r}{R})^2)} + \underbrace{\frac{\Delta r^2}{v_f^2}\frac{dV}{df}}_{O(1)} - \underbrace{\Delta r^2 f''}_{O(1)} - \underbrace{\Delta r^2 f'(2\gamma^3\ddot{R}\dot{R}^2 + R^{-1}\gamma^{-1})}_{O(\frac{\Delta r}{R})} = 0. \tag{171}$$

We can now clearly see that terms b and c are of leading order and terms a and d are suppressed.

This result provides a useful consistency check. Picking only leading order terms our EOM in the TWL for $O(2)\times O(2)$ symmetric bubbles is then

$$\frac{dV}{df} = v_f^2 f''. \tag{172}$$

Which is exactly the form of (103), and can be rewritten in the same way as

$$2V(f) = v_f^2 f'(\zeta)^2. \tag{173}$$

In particular, for our sextic potential, the solution of this equation is given by (52). Moreover (173) will be useful in computing the bounce action below.

4.2 Computing the Bounce Action of the Global String Case

In this section we aim to map the field-theoretic problem of finding an $O(2)\times O(2)$ symmetric solution $f(\rho,r)$ to a simpler quantum mechanics problem of finding the 'trajectory' of a single relativistic degree of freedom in some non-trivial potential. We begin our computation with the action in (155) by substituting $f(\zeta)$ in (153). We also perform substitutions for the $\frac{\partial\zeta}{\partial\rho}$ and $\frac{\partial\zeta}{\partial r}$ terms that we computed in (160) and (159) (where we take the expression before we apply the condition of being within the wall region). We then obtain

$$S_E^{2\times2} = 4\pi^2\int d\rho\rho\int drr\left[\frac{v_f^2}{2}\left(\frac{\partial f}{\partial\zeta}\right)^2\left[(\dot\gamma(r-R)-\gamma\dot R)^2+\gamma^2\right]+\frac{v_f^2n^2f^2}{2r^2}+V(f)\right]. \tag{174}$$

Since we are working in the TWL it makes sense to decompose the r integration into 3 regions: (i) The interior with $0<r<R(\rho)-\delta$; (ii) the wall where $R(\rho)-\delta<r<R(\rho)+\delta$ and (iii) the exterior with $R(\rho)+\delta<r<R_{Max}$, where δ is the wall thickness. We then have

$$\mathscr{L}^{2\times2} = \frac{v_f^2}{2}\left(\frac{\partial f}{\partial\zeta}\right)^2\left[(\dot\gamma(r-R)-\gamma\dot R)^2+\gamma^2\right]+\frac{v_f^2n^2f^2}{2r^2}+V(f), \tag{175}$$

and

$$S_E^{2\times2} = 4\pi^2\int d\rho\rho\Big(\int_0^{R(\rho)-\delta}drr[\mathscr{L}^{2\times2}]+\int_{R(\rho)-\delta}^{R(\rho)+\delta}drr[\mathscr{L}^{2\times2}] + \int_{R(\rho)+\delta}^{R_{Max}}drr[\mathscr{L}^{2\times2}]\Big). \tag{176}$$

We first evaluate the terms within the large parentheses and later will evaluate the ρ integration. We begin with the interior where the profile function f is constant and vanishing. Our only non-zero term is our potential,

$$\int_0^{R(\rho)-\delta} drr\left[\frac{v_f^2}{2}\left(\frac{\partial f}{\partial \zeta}\right)^2\left[(\dot{\gamma}(r-R)-\gamma\dot{R})^2+\gamma^2\right]+\frac{v_f^2 n^2 f^2}{2r^2}+V(f)\right]$$
$$=\int_0^{R(\rho)-\delta} drr\left[\frac{V(0)}{2}\right]=\left[-R^2(\rho)\frac{\Delta V}{2}\right]+O(\delta), \quad (177)$$

where ΔV was defined in (17). In other words, the interior integration gives rise to a negative volume term $\propto -\Delta V R^2$. As usual we drop terms of order δ. The wall region allows for the assumption $r = R$ in accordance with the TWL and we can use our results from (160) and (159) (now with the wall region simplifications). We find for the wall contribution

$$\int_{R(\rho)-\delta}^{R(\rho)+\delta} drr\left(\frac{v_f^2}{2}\left(\frac{\partial f}{\partial \zeta}\right)^2\left[(\dot{\gamma}(r-R)-\gamma\dot{R})^2+\gamma^2\right]+\frac{v_f^2 n^2 f^2}{2r^2}+V(f)\right)$$
$$=\frac{1}{2}\int_{R(\rho)-\delta}^{R(\rho)+\delta} dr\left(v_f^2\left(\frac{df}{d\zeta}\right)^2 R+\frac{v_f^2 n^2 f^2}{R}+2RV(f)\right). \quad (178)$$

Where we used that for $r = R$ the factor in the square brackets evaluates to 1 using the definition of γ in (154). Next we apply the substitution of our parameter ζ for a new differential element. We have from (160) that $\frac{\partial \zeta}{\partial r} = \gamma$ which we use to replace the differential element dr. We obtain

$$=\frac{v_f^2}{2}\int_{R(\rho)-\delta}^{R(\rho)+\delta} dr\left(\frac{n^2 f^2}{R}\right)+\frac{1}{2}\int_{-\delta\gamma}^{\delta\gamma}\frac{d\zeta}{\gamma}\left(v_f^2\left(\frac{df}{d\zeta}\right)^2 R+2RV(f)\right). \quad (179)$$

We take our EOM from (172), valid within the wall, and combine the last two terms giving

$$=\frac{v_f^2}{2}\int_{R(\rho)-\delta}^{R(\rho)+\delta} dr\left(\frac{n^2 f^2}{R}\right)+\frac{R}{\gamma}\int_{-\delta\gamma}^{\delta\gamma} d\zeta\, v_f^2\left(\frac{df}{d\zeta}\right)^2. \quad (180)$$

At this point we can see that the winding term, proportional to n^2, is relatively suppressed due to the $\left(\frac{df}{d\zeta}\right)^2$ term that is large within the wall region. Since f is bounded between 0 and 1, the winding term is of order δ, where δ denotes the wall thickness, and can be neglected. We previously defined the wall tension σ for the $O(3)\times\tau$ symmetric case in (57). We can use the same definition by replacing the parameter ρ with our parameter ζ and thus the last integral becomes

$$\frac{R}{\gamma}v_f^2\int_{-\delta\gamma}^{\delta\gamma} d\zeta\left(\frac{df}{d\zeta}\right)^2 = R\gamma^{-1}\sigma+O(\delta). \quad (181)$$

Lastly, for the exterior portion, $f = 1$ and all $\frac{df}{d\zeta}$ terms are 0 as well as $V(1) = 0$. We thus have

$$\frac{v_f^2}{2}\int_{R(\rho)+\delta}^{R_{Max}} dr\left(\frac{n^2 f^2}{r^2}\right)=v_f^2\int_{R(\rho)+\delta}^{R_{Max}} drr\left[\frac{n^2}{2r^2}\right]=\frac{v_f^2}{2}n^2\ln\left(\frac{R_{Max}}{R}\right)+O(\delta). \quad (182)$$

We can now proceed by substituting (181), (177) and (182) into (176), which yields

$$S_E^{2\times 2} = 4\pi^2 \Delta V \int d\rho \rho \left[\frac{v_f^2 n^2}{2\Delta V} \ln\left(\frac{R_{Max}}{R}\right) + \frac{\sigma}{\Delta V}\frac{R}{\gamma} - \frac{R^2(\rho)}{2} \right] + O(\delta), \tag{183}$$

where we pulled out a factor of ΔV. We would like to collect all parameter dependence into one parameter x. To that end, we begin by introducing a scaling factor α with

$$\tilde{\rho} = \frac{\rho}{\alpha} \qquad \text{and} \qquad \tilde{R} = \frac{R}{\alpha}, \tag{184}$$

to find

$$S_E^{2\times 2} = 4\pi^2 \Delta V \int d\tilde{\rho} \tilde{\rho} \alpha^2 \left[\frac{v_f^2 n^2}{2\Delta V} \ln\left(\frac{\tilde{R}_{Max}}{\tilde{R}}\right) + \alpha \frac{\sigma}{\Delta V}\frac{\tilde{R}}{\gamma} - \alpha^2 \frac{\tilde{R}^2(\rho)}{2} \right]. \tag{185}$$

If we set $\alpha = \frac{\sigma}{\Delta V}$ we are indeed left with a single parameter

$$x = \frac{2 v_f^2 n^2}{\Delta V \alpha^2} = \frac{2 n^2 v_f^2 \Delta V}{\sigma^2}. \tag{186}$$

To be explicit we find

$$S_E^{2\times 2} = 4\pi^2 \frac{\sigma^4}{\Delta V^3} \int d\tilde{\rho} \tilde{\rho} \left[\frac{x}{4} \ln\left(\frac{\tilde{R}_{Max}}{\tilde{R}}\right) + \frac{\tilde{R}}{\gamma} - \frac{\tilde{R}^2(\rho)}{2} \right]. \tag{187}$$

This action is one of the central results of this thesis. It has reduced the the problem of calculating the $O(2)\times O(2)$ bounce to the problem of solving the dynamics of a single degree of freedom $R(\rho)$ as a function of 'time' ρ. As a first check let us take the static limit $\dot{R} = 0$. In that case the EOM becomes

$$\frac{\delta L}{\delta \tilde{R}} = -\frac{x}{4}\frac{1}{\tilde{R}} + \underbrace{\frac{1}{\gamma}}_{\gamma=1} - \tilde{R} = 0. \tag{188}$$

We find the static string solution to be

$$\tilde{R}_s(x) = \frac{1-\sqrt{1-x}}{2}. \tag{189}$$

In the $O(4)$ case there is no seed containing the true vacuum like what we have here in the $O(2)\times O(2)$ symmetry, so there is $R_s = 0$ which we will see by sending the winding number $n \to 0$ and thus $x \to 0$ in (189). The final bounce action is then the difference

$$B^{2\times 2} = S_E^{2\times 2} - S_E^{2\times 2}\Big|_{\dot{R}=0}. \tag{190}$$

It evaluates to

$$B^{2\times 2} = 4\pi^2 \frac{\sigma^4}{\Delta V^3} \int d\tilde{\rho} \tilde{\rho} \left[\frac{x}{4} ln\left(\frac{\tilde{R}_s(x)}{\tilde{R}(\tilde{\rho})}\right) + \frac{\tilde{R}(\tilde{\rho})}{\gamma} - \frac{\tilde{R}^2(\tilde{\rho})}{2} - \tilde{R}_s(x) + \frac{\tilde{R}_s(x)^2}{2} \right]$$
$$\equiv 4\pi^2 \frac{\sigma^4}{\Delta V^3} \int d\tilde{\rho} g(\tilde{\rho}). \tag{191}$$

Where the function $g(\tilde{\rho})$ is a lagrangian. Solving analytically proved to be difficult thus we continue numerically after validating our results to the best of our ability.

4.3 Taking the Coleman Limit

The parameter x contains the winding number n. If we set x to approach 0 we should return to spherical symmetry (no winding) as the string becomes infinitely thin, $\tilde{R}_s(0) = 0$. We expect to recover our results from the Coleman bubble $O(3) \times \tau$ case. In this limit we can compute the action analytically as

$$B^{2\times 2}(x \to 0) = 4\pi^2 \frac{\sigma^4}{\Delta V^3} \int d\tilde{\rho}\tilde{\rho} \left[\frac{\tilde{R}(\tilde{\rho})}{\gamma} - \frac{\tilde{R}^2(\tilde{\rho})}{2} \right]. \tag{192}$$

We can begin by noting $\dot{\tilde{R}} = -\frac{\tilde{\rho}}{\tilde{R}(\tilde{\rho})}$, $\gamma = \frac{\tilde{R}(\tilde{\rho})}{\tilde{R}_c}$ and using the ansatz $\tilde{R}(\tilde{\rho}) = \sqrt{\tilde{R}_c^2 - \tilde{\rho}^2}$ corresponding to spherical symmetry. We evaluate with limits such that $\tilde{R}(\tilde{\rho}) \in \mathbb{R}$

$$\begin{aligned} B^{2\times 2}(x \to 0) = 4\pi^2 \frac{\sigma^4}{\Delta V^3} \int d\tilde{\rho}\tilde{\rho} \left[\tilde{R}_c - \frac{\tilde{R}_c^2 - \tilde{\rho}^2}{2} \right] \\ = 2\pi^2 \frac{\sigma^4}{\Delta V^3} \left[\tilde{R}_c \tilde{\rho}^2 - \frac{\tilde{R}_c^2 \tilde{\rho}^2}{2} + \frac{\tilde{\rho}^4}{4} \right]_0^{\tilde{R}_c}. \end{aligned} \tag{193}$$

We finally have

$$B^{2\times 2}(x \to 0) = 2\pi^2 \frac{\sigma^4}{\Delta V^3} \left[\tilde{R}_c^3 - \frac{\tilde{R}_c^4}{4} \right], \tag{194}$$

and we compute $\tilde{R}_c$ by varying the bounce,

$$\frac{\delta B^{2\times 2}(x \to 0)}{\delta \tilde{R}_c} = 0 \to \tilde{R}_c = 3, \tag{195}$$

which after the inverse rescaling in (184) yields the correct result from (86). Substituting back into (194), we finally obtain the bounce action, confirming that we return to the Coleman bubble in the $x \to 0$ limit

$$B^{2\times 2}(x \to 0) = \frac{27}{2}\pi^2 \frac{\sigma^4}{\Delta V^3}, \tag{196}$$

which indeed agrees with (87).

4.4 Numerical Bounce Solution

Our intermediate bounce action in (191) uses the dimensionless variables $\tilde{R}$ and $\tilde{\rho}$. We will henceforth drop the $\sim$ notation. We find an EOM for $R(\rho)$ by treating $g(\rho)$ in (191) as the new lagrange. Defined as

$$L_\rho = \rho \left(\frac{x}{4} log(\frac{1}{R(\rho)}) - \frac{R(\rho)^2}{2} + R(\rho)\gamma^{-1} \right), \tag{197}$$

where we define our γ as

$$\gamma = \frac{1}{\sqrt{1 + (\partial_\rho R(\rho))^2}}. \tag{198}$$

γ takes into account relativistic effects and thus the coordinate change of $t \to \rho$, including a spatial dimension generalizes from a point particle trajectory to the bubble wall trajectory. We can find the EOM explicitly from the above definitions by varying with respect to $R(\rho)$,

$$0 = -\rho\gamma + \frac{\rho x}{4R(\rho)} + R(\rho)\left(\rho + [\dot{R}(\rho) + \dot{R}^3(\rho) + \rho\ddot{R}(\rho)]\gamma^3\right). \tag{199}$$

We have defined our ρ in (145) where now we would like to write it in terms of our real time t as

$$\rho = \sqrt{z^2 - t^2}. \tag{200}$$

Evidently, this definition of ρ is only real in the region where $z^2 > t^2$. We would like to define a second $\hat{\rho}$ and solve our EOM again, now extending to the region where $z^2 \leq t^2$, to be explicit we set

$$\hat{\rho} = \sqrt{t^2 - z^2}. \tag{201}$$

Our new $R(\hat{\rho})$ is different to $R(\rho)$, we identify which one we refer to by the argument. The process for finding $R(\hat{\rho})$ is functionally the same, although we must compute a change of parameters to reflect $\rho = i\hat{\rho}$. The $\dot{R}$ terms in (197) and (199) for $R(\hat{\rho})$ will be taken with respect to the new $\hat{\rho}$. We use the conversion rule

$$\frac{d}{d\rho} = \frac{d}{d\hat{\rho}}\frac{d\hat{\rho}}{d\rho} = i\frac{d}{d\hat{\rho}}. \tag{202}$$

The EOM for $R(\hat{\rho})$ now can be written for our new regime in which $z^2 \leq t^2$, where the change is noted in the $\hat{\gamma}$ factor

$$\hat{\gamma} = \frac{1}{\sqrt{1 - (\partial_{\hat{\rho}} R(\hat{\rho}))^2}}. \tag{203}$$

We note that the change from ρ to $\hat{\rho}$ corresponds to an analytic continuation of $R(\rho)$ into the complex plane. Effectively, we solve $R(\rho)$ along the real $(t^2 < z^2)$ and imaginary $(z^2 \leq t^2)$ axis. Our lagrange for $R(\hat{\rho})$ is

$$L_{\hat{\rho}} = \hat{\rho}\left(\frac{x}{4} log(\frac{1}{R(\hat{\rho})}) - \frac{R(\hat{\rho})^2}{2} + R(\hat{\rho})\hat{\gamma}^{-1}\right), \tag{204}$$

which leads to the EOM

$$0 = -i\rho\hat{\gamma} + \frac{i\hat{\rho}x}{4R(\hat{\rho})} + R(\hat{\rho})\left(i\hat{\rho} + [i\dot{R}(\hat{\rho}) - i\dot{R}^3(\hat{\rho}) - i\hat{\rho}\ddot{R}(\hat{\rho})]\hat{\gamma}^3\right). \tag{205}$$

Our EOM in (199) and (205) could not be solved analytically, instead we opt for a numerical approach. Further, the two regions $t^2 < z^2$ and $z^2 \leq t^2$, must connect at $\rho \sim 0$. We would like this connection to be smooth and thus we proceed with linearized equations for $R(\rho)$ and $R(\hat{\rho})$ by making the ansatz

$$R_{\rho<<1}[\rho] = R_c + R_2\rho^2 \qquad \text{and} \qquad R_{\hat{\rho}<<1}[\hat{\rho}] = R_c + \hat{R}_2\hat{\rho}^2, \tag{206}$$

which assumes $R'(0) = 0$. We can use (199) and (205) to solve for R_2 and $\hat{R}_2$ respectively. We find that

$$R_2 = -\hat{R}_2 = \frac{4R_c - 4R_c^2 - x}{16R_c^2}. \tag{207}$$

This marks the end of what is analytically possible.

4.4.1 Shooting Algorithm

We proceed to solve for our functions $R(\hat{\rho})$ and $R(\rho)$ separately with Mathematica's `ParametricNDSolve` function. In addition we solve,

$$\frac{dB^{2\times2}(\rho)}{d\rho} = g(\rho), \tag{208}$$

which provides us with the Euclidian action B when evaluated for $\rho \to \infty$. We proceed by defining our boundary conditions for the numerical solutions to our equations. All of our boundary conditions lie in the $\rho << 1$ limit, making an analytic solution possible. The first is

$$B^{2\times2}(\rho = \rho_{min}) = \rho_{min}, \tag{209}$$

which follows from substituting (206) in (191). For our numerics we choose some $\rho_{min} \sim 10^{-12}$ and require (209).

The numerical solution requires boundary conditions that connect the linear solution in (206) as the numerical solutions at $\rho << 1$. These are defined as

$$R(\rho_{min}) = R_{\rho<<1}(\rho_{min}) \quad \text{and} \quad \dot{R}(\rho_{min}) = \dot{R}_{\rho<<1}(\rho_{min}), \tag{210}$$

where in the $R(\hat{\rho})$ regime the boundaries are the same. The remaining problem is that we don't know what the value for R_c is. We must find a critical radius for each value of x such that when we solve (191) for $R(\rho)$, the resulting function satisfies the asymptotic boundary condition

$$R(\rho \to \infty) = R_s(x), \tag{211}$$

where R_s is the radius of the metastable cosmic string defined in (189). However, for the numerical integration we must specify (210). We therefore use what is called a shooting algorithm, which allows us to find the value of R_c satisfying (211). To that end we impose our boundary conditions in (210) for some arbitrary choice of R_c and solve for the function $R(\rho)$ and $B^{2\times2}$ for a fixed choice of x. The algorithm with which we look for R_c is a series of two nested `for-loops` running only over our parametrized solution for $R(\rho)$, taking advantage of the fact that R_c will have the same value in the real and imaginary regimes. Our definition of the static radius function R_s in (189) determines the bounds for our x values. To be specific, $Rs(x)$ is only well defined for $0 \leq x \leq 1$. Our first `for-loop` runs over each x value from $x = 0.01$ to $x = 0.99$, where we are careful to avoid the marginal values of $x = 0$ and $x = 1$.

Within our first loop we set bounds for the range that R_c may be tested. We have $R_{Max} = 4$, $R_{min} = 0.01$ and an initial R_{temp} an arbitrary value between R_{min} and R_{Max}. The goal for our function is to find the value for R_c up to some precision (which we have chosen to be 10^{-7}) for which the $R(\rho)$ profile approaches the static string $R_s[x]$ and never crosses it. We use our parametrized $R(\rho)$ from our numerical solution and test the value R_{temp}. We take the minimum value of the wall profile and check if $R(\rho)$ dips below $R_s[x]$, in which case we have overshot, this is shown in Figure 4.2.

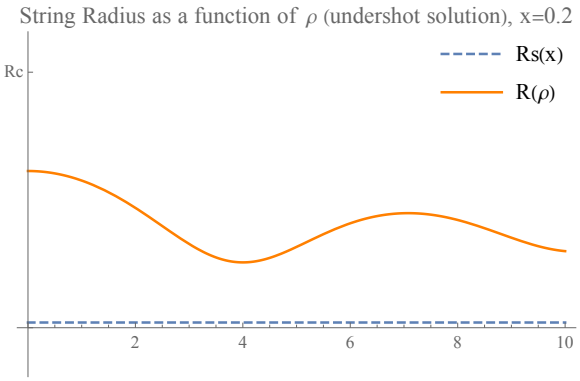

Figure 4.1. ρ-profile of undershooting solution when the guessed radius is smaller than the critical radius.

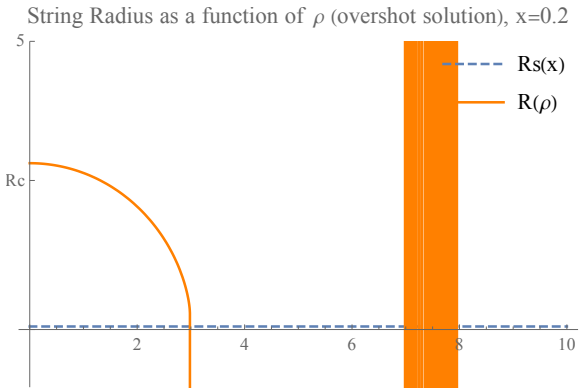

Figure 4.2. ρ-profile of overshooting solution profile when the guessed R_c is larger than the true R_c. The numerics breakdown at $7 < \rho < 8$.

Our check for overshooting is then

$$Overshooting = [R(\rho) - R_s[x] < 0 \text{ or } R(\rho) > 100], \tag{212}$$

where the second condition captures the numerical breakdown happening often in the overshooting case (also in Figure 4.2). We will discuss this special case more later. Undershooting is shown in Figure 4.1 where the $R(\rho)$ never crosses $R_s[x]$. When we have `overshoot = true`, we pick the new value for R_{Max} to be the current R_{temp} and then the new R_{temp} to mark the middle of the new interval between R_{min} and R_{Max}. In the case `overshoot = false` we perform an nearly identical process but updating R_{min} with R_{temp} and setting the new R_{temp} to mark the middle of this interval instead. Schematically, we therefore apply the following algorithm

$$\begin{aligned} If[Overshoot]: & \\ & R_{Max} = R_{temp} \\ & R_{temp} = [R_{Max} - R_{min}]/2 \\ Else: & \\ & R_{min} = R_{temp} \\ & R_{temp} = [R_{Max} - R_{min}]/2 \end{aligned} \tag{213}$$

When we find a value for R_{temp} that satisfies our precision choice and does not overshoot, we have found our complete solution.

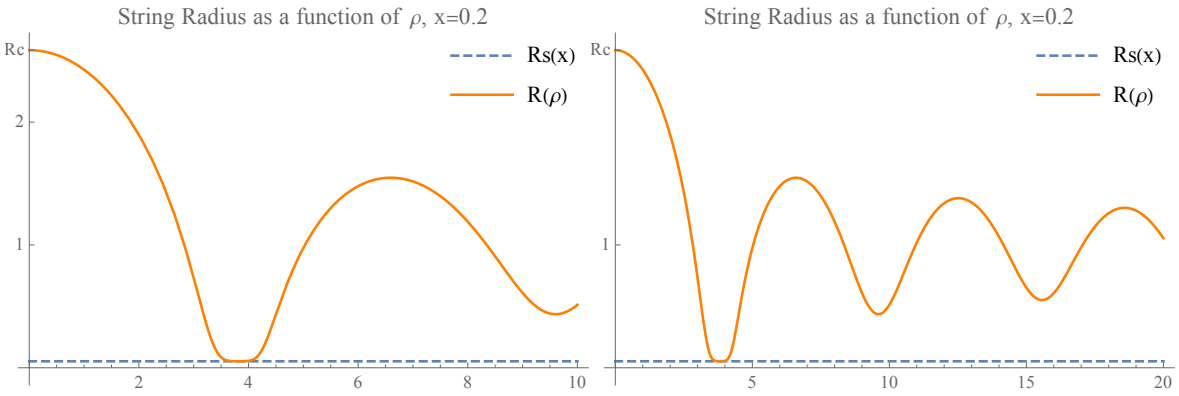

Figure 4.3. Partially converged profile solution. No cutoff has been applied, it is clear that the solution is only accurate up until it reaches the static string radius.

We have an example of a correct solution shown in Figure 4.3, one might observe that even in the best case our numerics break down after a certain point and we find the solution diverges again from our static radius, we attribute this behaviour to numerical uncertainties. This directs us to make some cutoff after which we will discard the rest of the numerical solution. In showing our results we only pick the portion of our solution up until its closest point to the static string radius, after which we simply connect it to $R_s[x]$ as a piecewise function, shown in Figure 4.4.

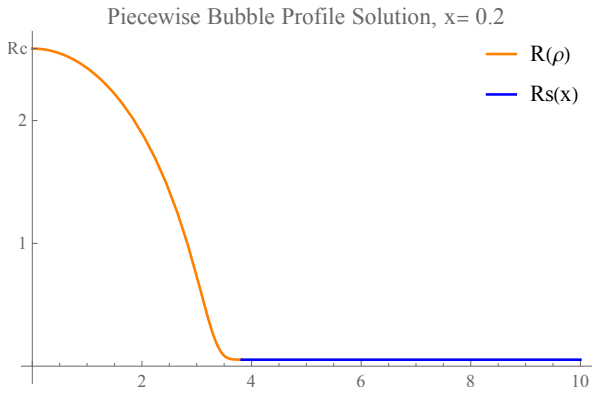

Figure 4.4. The initial solution is used until it reaches its minimum, at which point the function is transitioned into the x dependent static string solution.

We finally comment on a technical subtlety. We notice a numerical breakdown as well in the overshooting solution, see Figure 4.2. For some guesses of R_c we may see what appears to be undershooting as the profile does not pass $R_s[x]$, however, instead of continuing to oscillate smoothly as a truly undershot solution, the profile will grow extremely large as in Figure 4.5. This results in the extra condition in (212), $R(\rho) < 100$.

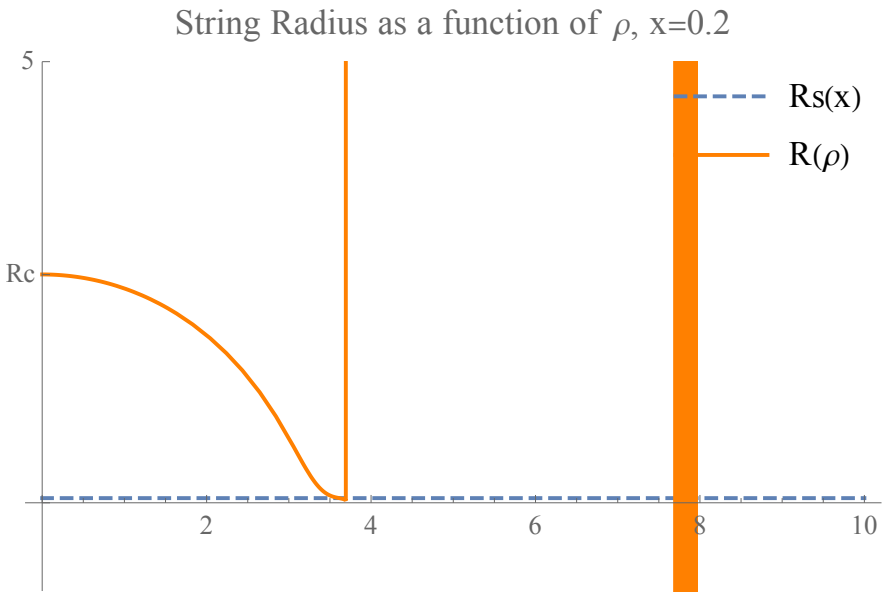

Figure 4.5. An overshot solution where $R(\rho)$ has a numerical breakdown.

4.4.2 Discussion of Numerical Results

In Figure 4.6 we see how as the parameter x increases the action decreases and the critical radius decreases as well. We can perform a fitting with `NonLinearModelFit` after normalizing both sets of data such that at $x = 0$, R_c and S_E are 1. We came up with the the following proxy functions

$$b(x) = (1 + a_1 x + a_2 x^2 + a_3 x^3 + a_4 x^4)(1-x)^{3/2}, \tag{214}$$

$$R_c(x) = \left(\frac{5}{6} + a_1 x + a_2 x^2 + a_3 x^3 + a_4 x^4\right)(1-x)^{1/2} + \frac{1}{6}. \tag{215}$$

We chose constants such that $S_E(x = 1) = 0$, in accordance with our analytic solution. We normalized our function such that $R_c(x = 0) = 1$ and the same normalization was applied to $R_s(x)$ for consistency. This meant that $R_s(1) = \frac{1}{6}$ which we use to fix the overall constant present in (215). The numerical fitting algorithm then gives the results in Table 4.1 for the

Table 4.1. Coefficient values for (214).

S_E	Estimate	Standard Error
a1	-0.685221	0.00915718
a2	2.36137	0.0718124
a3	-4.05758	0.170456
a4	2.68696	0.123367

case of the Euclidian action, and the results in Table 4.2 for the critical string radius.

Table 4.2. Coefficient values for (215).

R_c	Estimate	Standard Error
a1	-0.389933	0.00411724
a2	0.682105	0.025652
a3	-0.842578	0.0492224
a4	0.355474	0.0292485

Our results are depicted in Figure 4.6. They show that an increasing x value decreases the bounce action. Without considering the prefactor "A" momentarily, this shows an increased amplitude for vacuum tunneling with cosmic strings as a source as opposed to O(4) tunneling (corresponding to $x = 0$).

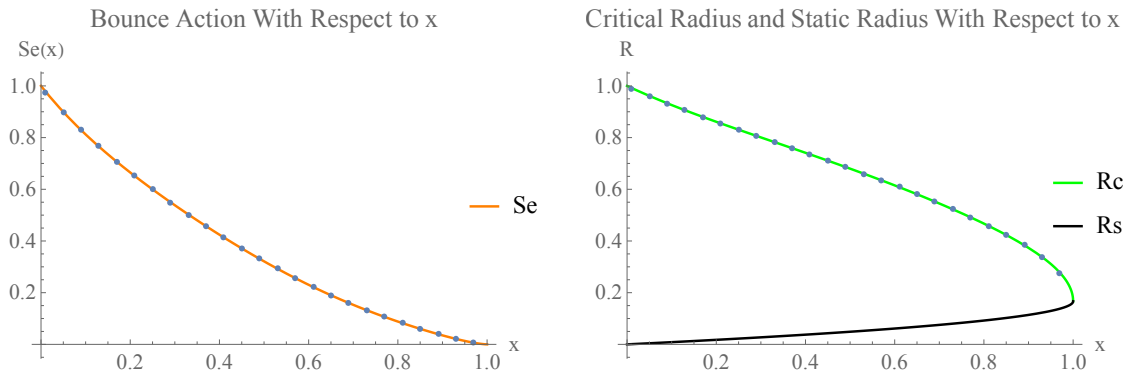

Figure 4.6. Functions described in Table 4.2, Table 4.1, (215) and (214) are shown as well as (189).

We shift our discussion to the actual bounce profiles of $R(\rho)$ and $R(\hat{\rho})$. The shape of the profile as a function of ρ is not obviously understandable, especially with the use of imaginary time. We use our definition of ρ to describe our profile as a function of z or t. The regions of ρ and $\hat{\rho}$ are joined together as a piecewise function. We can observe the profiles and see how the parameter x alters the shape of the bubbles.

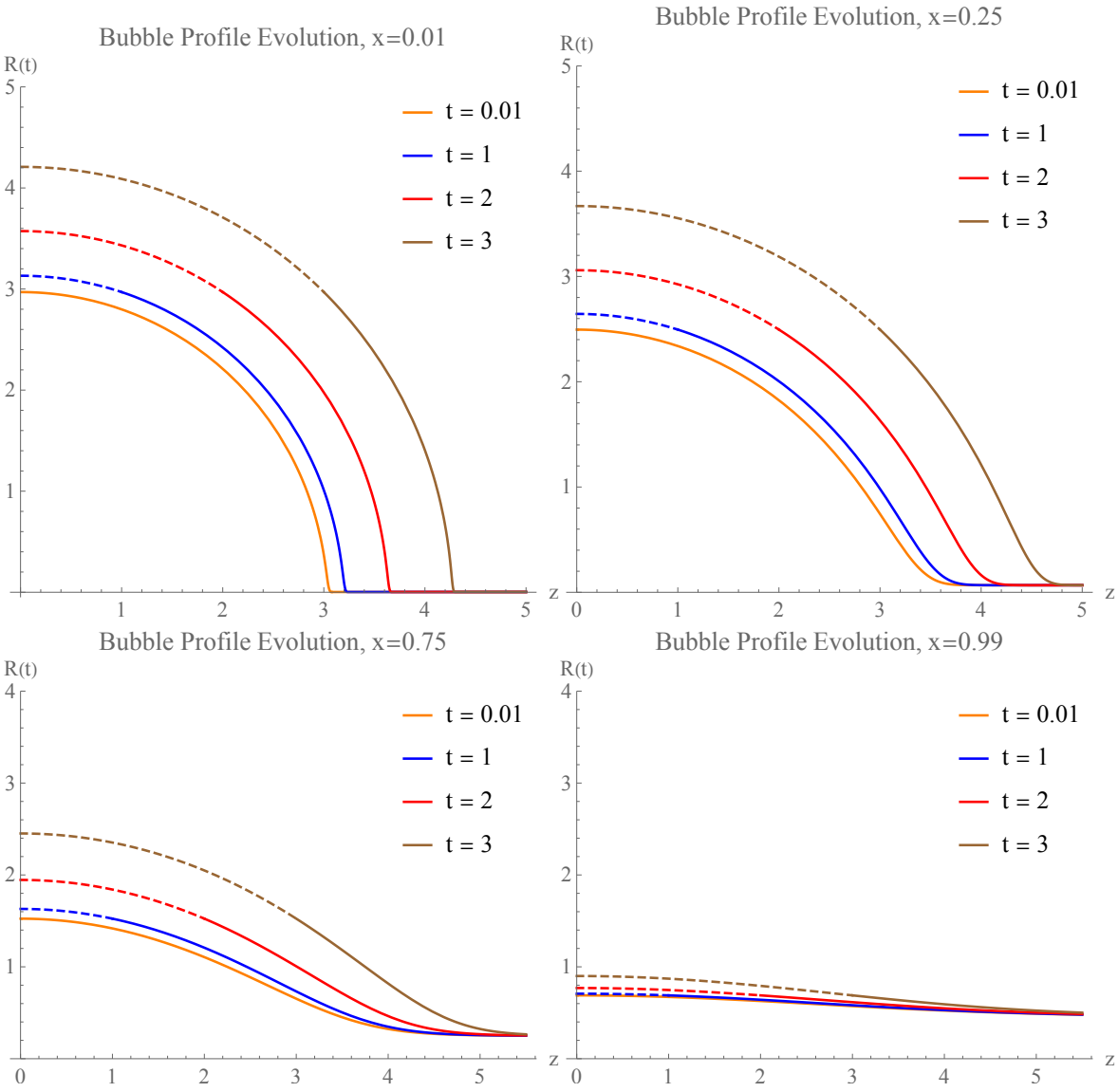

Figure 4.7. The shape of the bubble from a string for 3 different values of x. The solution transfers from $\hat{\rho}$ (Dashed) to ρ (Solid).

Our final results are shown in Figure 4.7. We observe the $R(\hat{\rho})$ solution noted by dashed lines smoothly continuing into the $R(\rho)$ solution. We see in the case of $x = 0.01$, the transition from the expanded part of the string to the metastable portion is abrupt, whereas for larger values of x the transition is far more smooth. We also note that for larger values of x the metastable string radius increases. One can imagine the physical representation of these string profiles by reflecting the image across the y-axis and then rotating it around the x-axis. This procedure gives rise to a cylindrically symmetric bulge. For larger x we find the shape of the bulge to be extremely subtle however the length along the string that the bubble occupies grows.

4.4.3 Wall Velocity Analysis

We will now extend our discussion and consider the trajectory and velocity of the bubble wall as time progresses. We can begin this by considering the plots of our solutions depicted

in Figure 4.4. Here we take discrete values of z and then consider the string radius R as a function of real time t. As before, dashed lines correspond to the region where $t^2 > z^2$ and the analytically continued solution with imaginary argument $\rho = i\hat{\rho}$ is relevant for describing the wall position. We see that in all cases the string core expands. The larger the value of z, the later this expansion sets in.

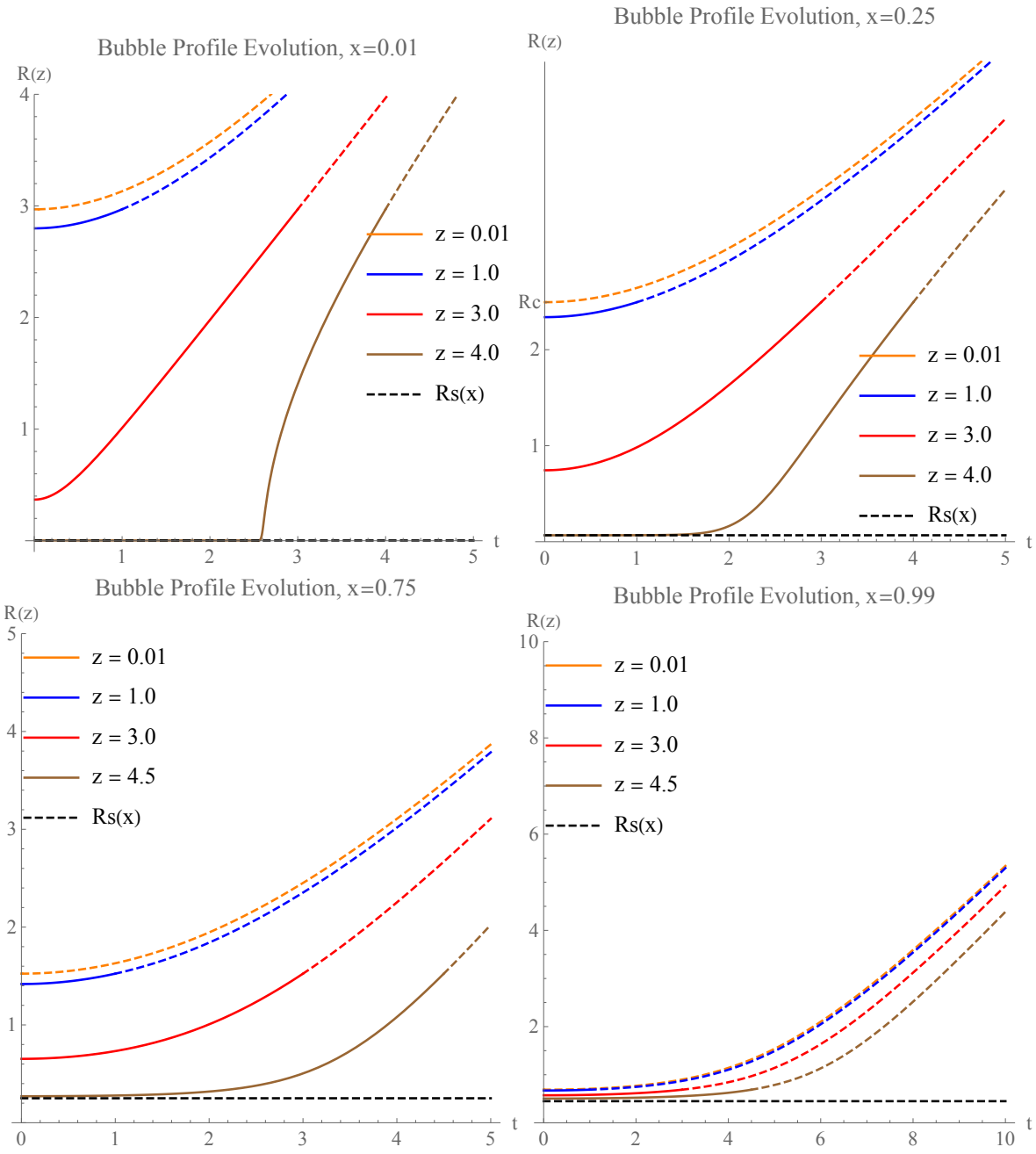

Figure 4.8. Trajectory of the bubble wall at location z on the string over time. The solution transfers from $\hat{\rho}$ (dashed) to ρ (solid).

We quickly see an issue for smaller values of x where the trajectory seems to be super-luminal. This is clear from the slope being greater than 1. We see for the largest parameter x the velocity of the wall quite reasonably approaches c. Comparing our equivalent parameter value

profiles in Figure 4.7, we see that the the position where the bubble transitions into the static string radius is the position in Figure 4.8 where the trajectory passes above 45°. We can confirm this observation by computing the time derivative of our solution.

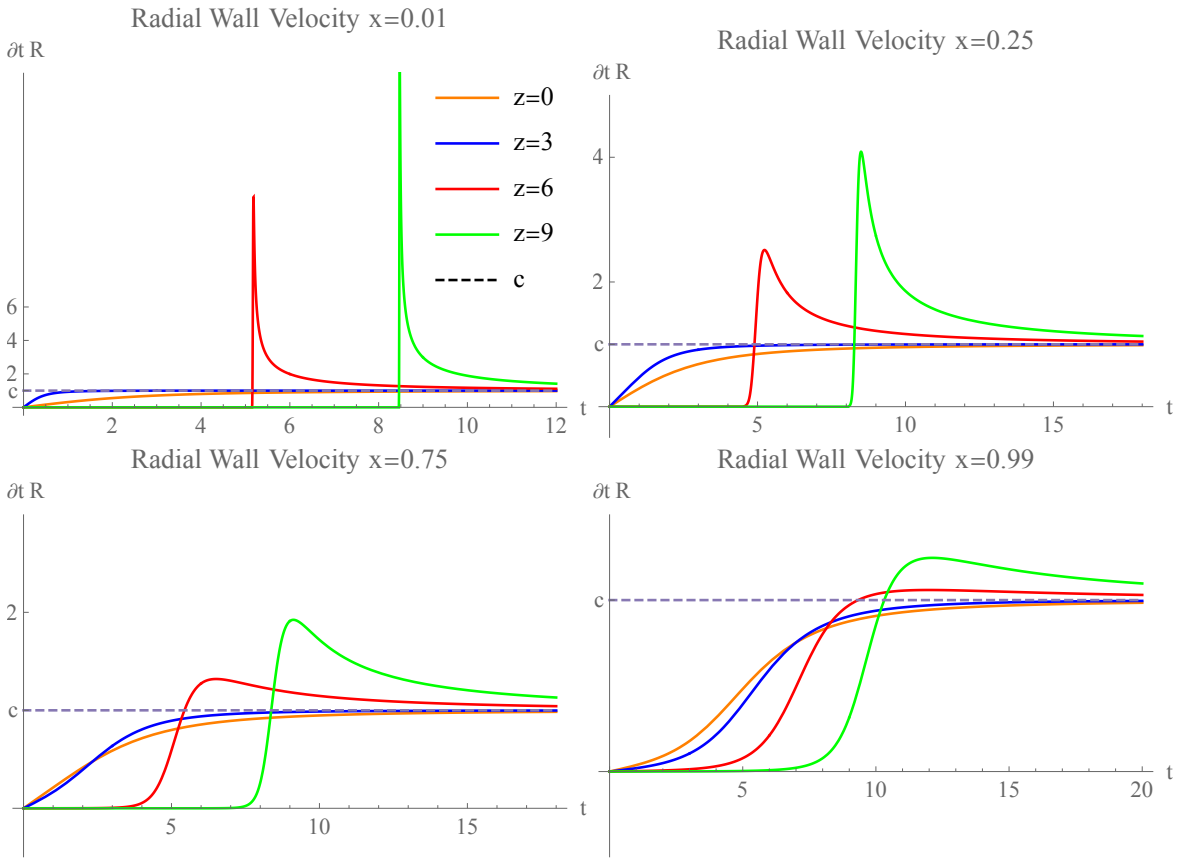

Figure 4.9. The above plots show the velocity of the bubble wall in the direction perpendicular to the length of the string at various distances from the position of nucleation. We see the velocity peaks above c and then slowly approaches c from above.

We can then see much clearer how a small parameter x results in a larger peak in velocity at the position along the length of the string where the radius is just beginning to expand. Does this really mean that the bubble wall is propagating at a superluminal velocity? We will argue that this is not the case. Instead, this result is a consequence of our oversimplified method of computing the velocity of the bubble. In Figure 4.10 we consider two time slices of a bubble expansion. We observe the position of the wall at $t = 0.5$ (red) and $t = 2$ (blue) and visualize what we are plotting in Figure 4.9 in terms of the dashed vertical lines. The $\partial_t R$ vector connects two patches on the bubble surface—these two patches are not equivalent. In our most exaggerated case the shape of the bubble is approximately that of a sphere. We can segment the bubble into regions of width $z = 1$, and as we approach the edge of the bubble, the length of wall contained grows.

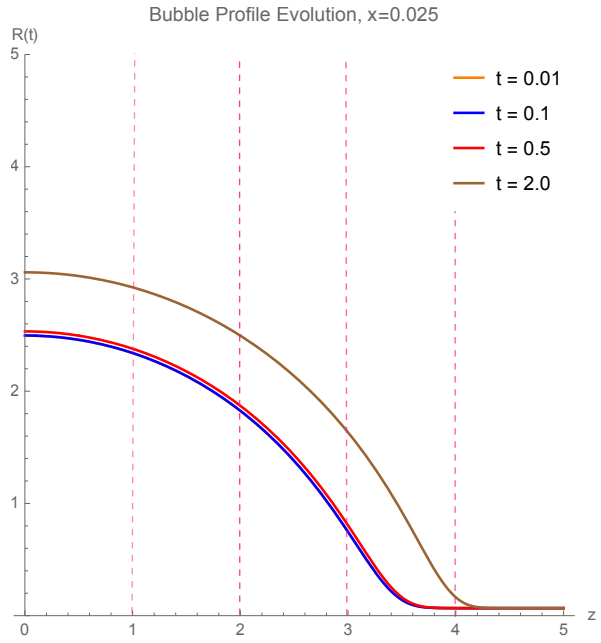

Figure 4.10. The orange dashed lines are placed at equal intervals along the length of the string. This illustrates that the dynamics of the wall are highly dependent on the z position of the string segment.

Clearly, we must take a more careful approach in discussing different regions of the wall along the z axis. As we look further from the axis of symmetry at $z = 0$ the velocity vector from two equivalent patches accumulates a change in the z direction. To account for this change we can compute the projection of our velocity onto the normal of the surface.

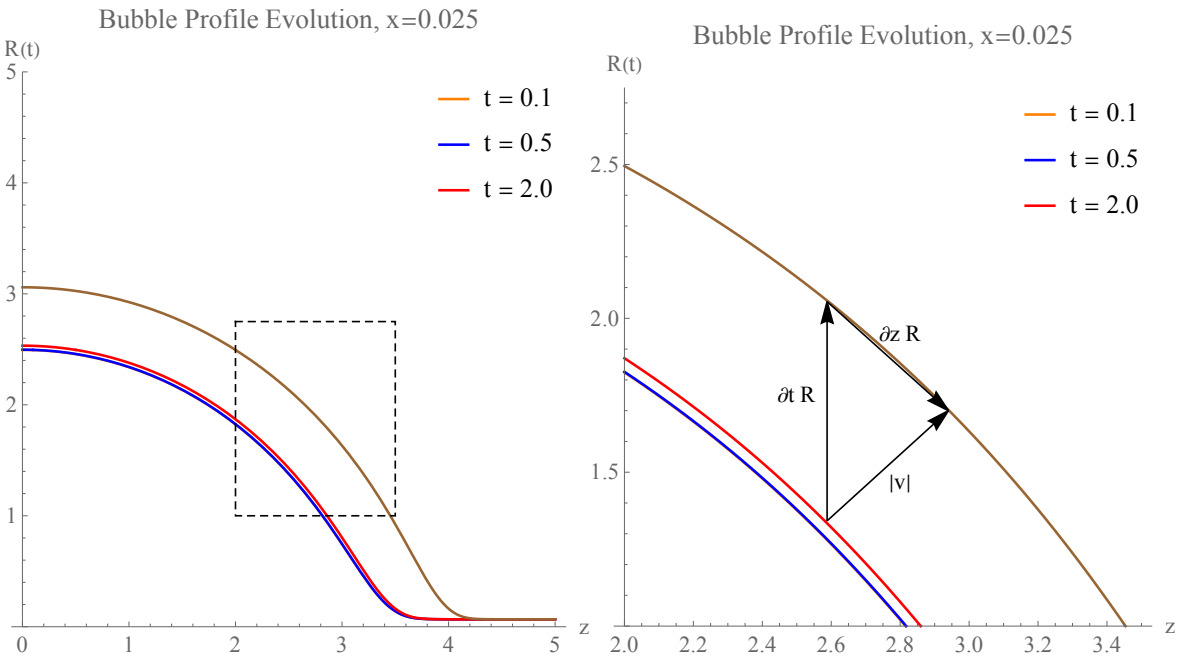

Figure 4.11. In the left hand plot we see a bubble profile with the dashed box highlighting the area shown on the right. The arrows denote the vectors found by simply differentiating with respect to t or z whereas $|v|$ shows the true trajectory of a patch on the bubble wall.

If we observe a patch on the wall at $z = 0$ it is trivial that any acceleration will occur in the radial direction as it lies exactly on the center of z symmetry. If we however observe a patch some distance in one direction, say at $z = 2.6$ in Figure 4.11, as the bubble expands this patch has an acceleration in the z direction as well as in the radial direction. To find the actual expansion rate in terms of the radius of the bubble, we must project $\partial_t R$ onto the normal of the surface. To begin, we identify the slope of the bubble surface to be $\partial_z R$. The normal of the surface forms a triangle with the vector $\partial_z R$. We can decompose the triangle to find the component from of the normal vector $\hat{n}$. To make this more explicit, we first define the normal vector as

$$\hat{n} = \left(\frac{1}{\sqrt{1+\partial_z R^2}}, \frac{\partial_z R}{\sqrt{1+\partial_z R^2}} \right). \tag{216}$$

It is straightforward to check that the normal vector $\hat{n}$ has unit length. The normal projection is then given by

$$\hat{n} \cdot \partial_t R = \left(\frac{\partial_t R}{\sqrt{1+\partial_z R^2}}, 0 \right), \tag{217}$$

and we define correspondingly

$$|\vec{v}(t,z)| = \frac{\partial_t R}{\sqrt{1+(\partial_z R)^2}}. \tag{218}$$

With this adjustment we can correct the velocity profiles such that they behave physically as in Figure 4.12.

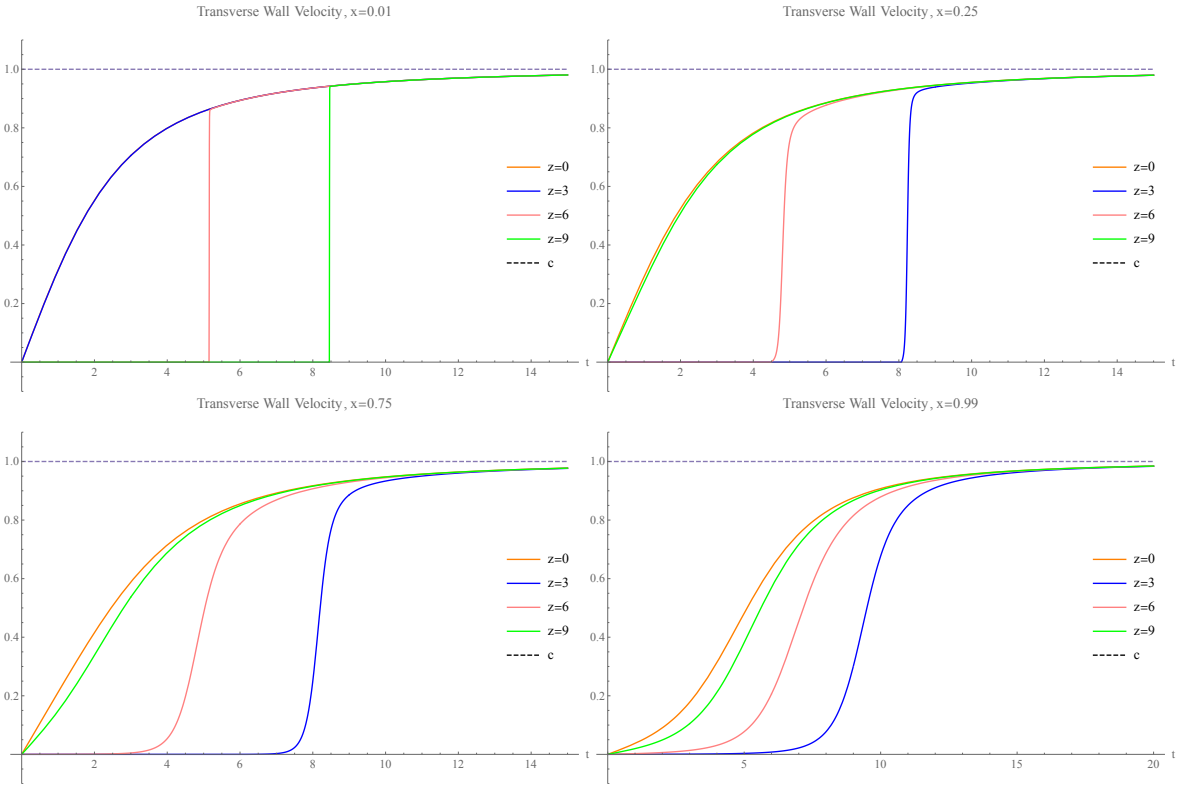

Figure 4.12. Acceleration of a patch of wall located initially at various positions along the string.

With our adjustment we have been able to show that the bubble expansion is in fact subluminal and thus behaves physically. Even for very small x values we see that the velocity of any patch on the expanding string wall asymptotically approaches c.

4.5 Phenomenology

At this point we would like to contextualize our findings and discuss possible applications. In order to do this we require some knowledge of the prefactor, the form of which is computed for the $O(4)$ case in [2]. The resulting amplitude with all terms is written

$$\gamma_0 = \frac{\Gamma_0}{V} = \left(\frac{B_0}{2\pi}\right)^2 \left[\frac{det'[-\partial^2 + V'']}{det[-\partial^2 + V''_+]}\right]^{-1/2} e^{-B_0}, \tag{219}$$

where V''_+ is the potential at the false minimum and V'' is at any point in the field. Here the prefactor is made up of two components, let us first discuss the term $\left(\left(\frac{B[\phi]}{2\pi}\right)^{1/2}\right)^4$. The exponential of 4 is representative of the directions of symmetry in the bounce action. That is to say, the action is invariant under translations in the t, x, y, z directions. We see that each symmetry gains a factor of $\left(\frac{B[\phi]}{2\pi}\right)^{1/2}$. This term itself is dimensionless as is the bounce action B_0 from (63).

The second term requires some more tact. Considering the symmetries of our $O(4)$ bounce action, we again observe that the action is invariant under four directions of variation, each of these will result in a vanishing eigenvalue. The $'$ included in the numerator signifies the omission of any vanishing eigenvalues (of which we have 4). Let us compute the mass dimensions of the term, beginning with $[det[-\partial^2 + V''_+]] = (M^{-2})^\beta$. Where β is the length of the diagonal. We find the numerator to have $[det'[-\partial^2 + V'']] = (M^{-2})^{\beta-4}$. Our ratio of determinants then has mass dimension $M^{-2(\beta-4-\beta)} = M^8$. We find that the mass dimensions of the prefactor are M^{-4}. We take the result from [36] and write our prefactor replacing each mass dimension with a factor R_c,

$$\gamma_0 = \frac{\Gamma_0}{V} \sim \left(\frac{B_0}{2\pi}\right)^2 \left[\frac{1}{R_c^4}\right] e^{-B_0}. \tag{220}$$

We now consider our unique case of the modified cylindrical symmetry, we find that there are now only 2 directions of stability in the solution (t, z) and thus we have a new rate of nucleation for such a case written

$$\frac{\Gamma_s}{L_s} = \left(\frac{B_s[\phi]}{2\pi}\right) \left[\frac{det'[-\partial^2 + V'']}{det[-\partial^2 + V''_+]}\right]^{-1/2} e^{(-[B_s[\phi]])} \sim \left(\frac{b(x)B_0}{2\pi}\right) \left[\frac{1}{R_c^2}\right] e^{-B_0 b(x)}. \tag{221}$$

We have that Γ_s is the nucleation rate per Hubble patch and $L_s = H_s^{-1}$ the average length of a string in a Hubble patch. Here the nucleation rate $\frac{\Gamma_s}{L_s}$ describes the rate per unit length of the string, as opposed to the $O(4)$ case, which is per unit volume. Let us determine the order of magnitude of the prefactor. Considering the symmetries of our bounce, a modified cylinder,

we find two directions in which we can vary the action and conserve its value, those are τ and z. These will resolve in 2 vanishing eigenvalues for the $det'[-\partial^2 + V'']$ term. Where in the $O(4)$ case we had a dimensionality of M^{-4} for the prefactor. In the $O(2) \times O(2)$ case we take the dimensionality to be M^{-2} where the exponent is directly proportional to the number of 0 eigenvalues.

For both the $O(4)$ and $O(2) \times O(2)$ cases there is a negative eigenvalue in the determinant. This corresponds to the value of R_c, which when varied increases the magnitude of the bounce action. The negative eigenvalues must be dealt with carefully as done in [2].

We introduce N_s, representing the number of Hubble length open strings found per Hubble patch, we write $L_s = N_s l_s$ where l_s is one Hubble length. We would like to directly compare the tunneling rates of γ_0 and γ_s, to do so we must adjust such that we have $\gamma_s = \frac{\Gamma_s}{V}$, nucleation rate per Hubble patch

$$\frac{\Gamma_s}{V} = \frac{\Gamma_s}{L_s}\frac{N_s l_s}{V}. \tag{222}$$

We have said that there is average length of string L_s per Hubble patch (with volume $V = H_s^{-3}$). We can then write

$$\gamma_s = \frac{\Gamma_s}{V} = \left(\frac{b(x)B_0}{2\pi}\right)\left[\frac{N_s H_s^2}{R_c^2}\right] e^{-B_0 b(x)}. \tag{223}$$

This $\gamma_{0,s}$ marks the tunneling probability per unit volume ($V = H_{0,s}^{-3}$) and Hubble time ($t = H_{0,s}^{-1}$). In order to compare the overall tunneling contributions, H_s and H_0 which note the inverse lifetime of the vacuum. We can find this lifetime ($t_{0,s}$) by multiplying the tunneling amplitude per unit volume $\gamma_{0,s}$ by Hubble volume (H^{-3}). We choose $t_{0,s}$ to be the lifetime of the vacuum and t_{age} the age of the universe, written as

$$t_{0,s} = \frac{1}{\Gamma_s} = \frac{1}{V\gamma_{0,s}} = \frac{1}{H_{0,s}^{-3}\gamma_{0,s}}, \tag{224}$$

and

$$t_{age} = \frac{1}{H}. \tag{225}$$

If we choose $t_{0,s} = t_{age}$ we can define the decay rate nicely as

$$H_{0,s}^4 = \gamma_{0,s}. \tag{226}$$

To find the conditions under which cosmic string decay dominates the rate of vacuum decay we need $t_s < t_0$ written as

$$\frac{\Gamma_s}{\Gamma_0} > 1 \rightarrow \frac{H_s}{H_0} > 1. \tag{227}$$

We can write H_s and H_0 from our γ_0 and γ_s definitions and our relationship from (220), (223) and (226) respectively. For the $O(2) \times O(2)$ case we have

$$\gamma_s = H_s^4 = \left(\frac{b(x)B_0}{2\pi}\right)\left[\frac{N_s H_s^2}{R_c^2}\right] e^{-B_0 b(x)}, \tag{228}$$

eliminating a factor of H_s^2 and taking the square root, we find

$$H_s = \frac{\sqrt{b(x)B_0N_s}}{R_c\sqrt{2\pi}}e^{-\frac{1}{2}B_0b(x)}. \tag{229}$$

For the $O(4)$ decay we find

$$\gamma_0 = H_0^4 = \left(\frac{B_0}{2\pi}\right)^2\left[\frac{1}{R_c^4}\right]e^{-B_0}, \tag{230}$$

and then

$$H_0 = \frac{\sqrt{B_0}}{R_c\sqrt{2\pi}}e^{-\frac{1}{4}B_0}. \tag{231}$$

We can then write the condition

$$1 < \frac{H_s}{H_0} = \sqrt{N_sb(x)}e^{-\frac{1}{4}B_0(2b(x)-1)}. \tag{232}$$

We translate this condition into some bounds on $b(x)$. Taking $N_s \sim 1$ as the assumed number of cosmic strings per Hubble patch, we find $b(x) \leq \frac{1}{2}$ to conserve our condition in (232). We can see from (214) and Figure 4.6 that our bounds on x are

$$0.4 \leq x \leq 1. \tag{233}$$

This inequality, one of the main results of the project, shows actual applicable constraints on the conditions in which this decay is possible.

5 Conclusion

We began our project with two main goals. First, computing a new bounce solution corresponding to the nucleation of a bubble configuration describing the expansion of a metastable cosmic string in the TWL, where the core of the string sits in the true vacuum and the outside of the string in the false vacuum. Our second question was how does the tunneling rate of this $O(2) \times O(2)$ symmetric bounce solution compare to the previously discussed $O(4)$ symmetric Coleman bounce. On the path to answering our two main questions we must confirm a selection of equivalences and estimations. In computing the bounce for the $O(2) \times O(2)$ symmetry in the TWL, we write an ansatz for the field as the Lorentz-boosted thin wall profile. However before solving the more difficult $O(2) \times O(2)$ bounce, we took a step back and considered the conventional case of the spherical bubble. Here our first task was computing the action of the $O(3) \times \tau$ symmetry with the same Lorentz boost and confirming that this is equivalent to the $O(4)$ symmetric case, both again in the TWL. This was confirmed in (63) and (87). In our computations we take the TWL to mean that in the EOM (51) the "friction term" vanishes in the wall region. It is this condition that leads us to our equivalence. We prove this to be true when the height of the potential barrier is much larger than the difference of potentials between the true and false minima. We also show that within the wall region, the friction term is very small and the kinetic and potential terms in the EOM are each independently larger than the friction term.

In Section 3, we reviewed the $O(2)$ symmetric cosmic string. With such a symmetry we acquire a new winding contribution, controlled by the winding number n, and write two new ansatz for the gauge field a (109) and scalar field f (106). We evaluate the EOM for such a symmetry and find (128), (127). We find in accordance with the literature, that the local case results in a magnetic flux through the core of the string and most importantly vanishing energy outside of the string. The global case, found by setting the gauge field $a = 0$ everywhere, results in a diverging energy outside of the string regularized by the string separation scale. We continue by describing the string tension μ in terms of the wall tension σ and then describe a derivation of the deficit angle around a cosmic string. A brief discussion of astrophysical effects from the cosmic string follows. While this section provided mostly a review on cosmic strings, as a non-standard technique not commonly discussed in the literature we used the TWL to describe the strings.

Finally we arrive at our computation of the bounce action for $O(2) \times O(2)$ symmetric bubbles. We choose to proceed in the global case out of simplicity. However the local case has been computed in follow up work in [31]. The EOM in the global case is (164) where there is a winding term and a friction term. This equation is valid in the wall region (172). We compute the action to find a bounce action with a single parameter dependence (191), given by x. As one of our main results we provide a semi-analytic proxy for the bounce action as a function of x. We analytically verify the validity of this up to the $x \to 0$ limit. We expect to return to the $O(4)$ symmetric result, which we do in (196). We find the bounce action to decrease with an increased x parameter, this is interpreted as an increased tunneling probability as the

bubble shape is less spherical and instead more oblong with a preexisting vacuum sitting at the center. These results are shown in Figure 4.6, and the bubble profile in Figure 4.7. Our last results follow from a numerical evaluation of the action over the τ, z coordinates and find a solution $R(\rho)$ for the profile of the bubble. We spent some time showing the wall velocity of our bubble does not reach any impossible values. We analyzed the shape of the wall profile in Figure 4.11 and found the actual velocity of a section of the wall in (218). We finally determine the trajectory of the bubble expansion shown in Figure 4.12.

Our final phenomenology discussion considers the lifetime of the vacuum. We found some bounds (233) where a vacuum containing a string defect is more likely to decay via the string core tunneling than the Coleman vacuum tunneling. We consider the prefactor and its contribution to the overall tunneling rate for our broken symmetry compared to the spherical symmetry. The main result being (233) defining the bounds on our parameters where the cosmic string tunneling will dominate the total tunneling rate.

An interesting result from this research is the particular mechanism for string decay and its consequences for the stochastic GW signal produced by these decaying strings. We might refer to the results from the 15 year NANOGrav pulsar timing array data set [48], where the authors detect stochastic GW signals over a range of nano-Hertz frequencies. Their results show a decreased strength in signal at lower frequencies. However a signal from a network of local-strings, produced from cusps, oscillating loops and kinks, leads to an approximately constant power spectrum, incompatible with the increasing slope. If we are to take these results at face value, they eliminate the possibility for local strings to exist at all at late times provided the string tension is not much smaller than the GUT scale, ie: $<< 10^{15} GeV$ [48]. The decay mechanism discussed is one possible explanation for this discrepancy. The strings could exist at early times but be eliminated in the phase transition discussed here, suppressing the GW signals at later times and smaller frequencies. This cutoff can be accounted for by any string decay mechanism at a certain point in time, for example the earlier mentioned monopole-antimonopole decay from [36], where the decay of the strings will suppress the GW signal at late times [49–52]. Moreover as was discussed in [31], the bubbles from the cosmic string seeding discussed here are not spherical[1]. This would result in a GW signal distinct from those produced by other sources such as Coleman bubble vacuum decay. In particular, a single Coleman bubble due to its spherical geometry has vanishing quadrupole moment and does not emit GW except during bubble collisions [53].

Cosmic strings are very interesting objects that have recently been gaining interest. Our topic can be explored further, the tunneling rate of the local string with fully relativistic expansion has yet to be described. We use the TWL frequently to simplify calculations however the omission of this simplification could be explored. A phase transition such as the one we discussed release energy, this in particular is one of the theorized ways to resolve the Hubble tension [54]. As mentioned previously the nonspherical bubbles lead to unique GW signals which one can look for in pulsar-timing arrays [31, 55]. Overall there remains much to be explored in the topic of seeded phase transitions, we can only look forward to learning more.

[1]The cited paper focuses on the local cosmic string in it's GW discussion, whereas this thesis focuses on the global string and does not discuss GW production.

References

1. Coleman, S. R. The Fate of the False Vacuum. 1. Semiclassical Theory. *Phys. Rev. D* **15.** [Erratum: Phys.Rev.D 16, 1248 (1977)], 2929–2936 (1977).
2. Callan Jr., C. G. & Coleman, S. R. The Fate of the False Vacuum. 2. First Quantum Corrections. *Phys. Rev. D* **16,** 1762–1768 (1977).
3. Bödeker, D. & Buchmüller, W. Baryogenesis from the weak scale to the grand unification scale. *Rev. Mod. Phys.* **93,** 035004. https://link.aps.org/doi/10.1103/RevModPhys.93.035004 (3 Aug. 2021).
4. Giudice, G. F., Lee, H. M., Pomarol, A. & Shakya, B. Nonthermal heavy dark matter from a first-order phase transition. *JHEP* **12,** 190. arXiv: 2403.03252 [hep-ph] (2024).
5. Shakya, B. Aspects of particle production from bubble dynamics at a first order phase transition. *Phys. Rev. D* **111,** 023521. arXiv: 2308.16224 [hep-ph] (2025).
6. Niedermann, F. & Sloth, M. S. New early dark energy. *Phys. Rev. D* **103,** L041303. arXiv: 1910.10739 [astro-ph.CO] (2021).
7. Caprini, C. & Figueroa, D. G. Cosmological Backgrounds of Gravitational Waves. *Class. Quant. Grav.* **35,** 163001. arXiv: 1801.04268 [astro-ph.CO] (2018).
8. Copeland, E. J., Pogosian, L. & Vachaspati, T. Seeking String Theory in the Cosmos. *Class. Quant. Grav.* **28,** 204009. arXiv: 1105.0207 [hep-th] (2011).
9. Sakellariadou, M. Cosmic Strings and Cosmic Superstrings. *Nuclear Physics B - Proceedings Supplements* **192-193.** Theory and Particle Physics: The LHC Perspective and Beyond, 68–90. ISSN: 0920-5632. https://www.sciencedirect.com/science/article/pii/S0920563209005544 (2009).
10. Nielsen, H. & Olesen, P. Vortex-line models for dual strings. *Nuclear Physics B* **61,** 45–61 (Sept. 1973).
11. Hindmarsh, M. B. & Kibble, T. W. B. Cosmic strings. *Rept. Prog. Phys.* **58,** 477–562. arXiv: hep-ph/9411342 (1995).
12. Silk, J. & Vilenkin, A. Cosmic strings and galaxy formation. *Phys. Rev. Lett.; (United States)* **53:17.** ISSN: ISSN PRLTA. https://www.osti.gov/biblio/6259970 (Oct. 1984).
13. Jiao, H., Brandenberger, R. & Refregier, A. Early structure formation from cosmic string loops in light of early JWST observations. *Phys. Rev. D* **108,** 043510. arXiv: 2304.06429 [astro-ph.CO] (2023).
14. Moss, I. G. Black-hole bubbles. *Phys. Rev. D* **32,** 1333–1344. https://link.aps.org/doi/10.1103/PhysRevD.32.1333 (6 Sept. 1985).
15. Gregory, R., Moss, I. G. & Withers, B. Black holes as bubble nucleation sites. *JHEP* **03,** 081. arXiv: 1401.0017 [hep-th] (2014).
16. Shkerin, A. & Sibiryakov, S. Black hole induced false vacuum decay from first principles. *JHEP* **11,** 197. arXiv: 2105.09331 [hep-th] (2021).
17. Mukaida, K. & Yamada, M. False Vacuum Decay Catalyzed by Black Holes. *Phys. Rev. D* **96,** 103514. arXiv: 1706.04523 [hep-th] (2017).

18. Arnold, P. B. GRAVITY AND FALSE VACUUM DECAY RATES: O(3) SOLUTIONS. *Nucl. Phys. B* **346,** 160–192 (1990).
19. Berezin, V. A., Kuzmin, V. A. & Tkachev, I. I. O(3) Invariant Tunneling in General Relativity. *Phys. Lett. B* **207,** 397–403 (1988).
20. Billam, T. P., Gregory, R., Michel, F. & Moss, I. G. Simulating seeded vacuum decay in a cold atom system. *Phys. Rev. D* **100,** 065016. arXiv: 1811.09169 [hep-th] (2019).
21. Jinno, R., Kume, J. & Yamada, M. Super-slow phase transition catalyzed by BHs and the birth of baby BHs. *Phys. Lett. B* **849,** 138465. arXiv: 2310.06901 [hep-ph] (2024).
22. Steinhardt, P. J. Monopole Dissociation in the Early Universe. *Phys. Rev. D* **24,** 842 (1981).
23. Steinhardt, P. J. Monopole and Vortex Dissociation and Decay of the False Vacuum. *Nucl. Phys. B* **190,** 583–616 (1981).
24. Agrawal, P. & Nee, M. The Boring Monopole. *SciPost Phys.* **13,** 049. arXiv: 2202.11102 [hep-ph] (2022).
25. Kumar, B., Paranjape, M. B. & Yajnik, U. A. Fate of the false monopoles: Induced vacuum decay. *Phys. Rev. D* **82,** 025022. arXiv: 1006.0693 [hep-th] (2010).
26. Blasi, S. & Mariotti, A. Domain Walls Seeding the Electroweak Phase Transition. *Phys. Rev. Lett.* **129,** 261303. arXiv: 2203.16450 [hep-ph] (2022).
27. Agrawal, P., Blasi, S., Mariotti, A. & Nee, M. Electroweak phase transition with a double well done doubly well. *JHEP* **06,** 089. arXiv: 2312.06749 [hep-ph] (2024).
28. Kamada, A. & Yamada, M. Gravitational wave signals from short-lived topological defects in the MSSM. *JCAP* **10,** 021. arXiv: 1505.01167 [hep-ph] (2015).
29. Lee, B.-H. *et al.* Battle of the bulge: Decay of the thin, false cosmic string. *Physical Review D* **88.** ISSN: 1550-2368. http://dx.doi.org/10.1103/PhysRevD.88.105008 (Nov. 2013).
30. Dasgupta, I. Vacuum tunneling by cosmic strings. *Nuclear Physics B* **506,** 421–435. ISSN: 0550-3213. http://dx.doi.org/10.1016/S0550-3213(97)00546-4 (Nov. 1997).
31. Chatrchyan, A., Niedermann, F. & Richman-Taylor, P. String-induced vacuum decay. arXiv: 2510.27579 [astro-ph.CO] (Oct. 2025).
32. Hiscock, W. A. Nucleation of vacuum phase transitions by topological defects. *Physics Letters B* **366,** 77–81. ISSN: 0370-2693. http://dx.doi.org/10.1016/0370-2693(95)01345-8 (Jan. 1996).
33. Lee, B.-H. *et al.* Tunneling decay of false vortices. *Phys. Rev. D* **88,** 085031. https://link.aps.org/doi/10.1103/PhysRevD.88.085031 (8 Oct. 2013).
34. Vilenkin, A. Cosmological evolution of monopoles connected by strings. *Nuclear Physics B* **196,** 240–258. ISSN: 0550-3213. https://www.sciencedirect.com/science/article/pii/0550321382900372 (1982).
35. Buchmuller, W., Domcke, V. & Schmitz, K. Metastable cosmic strings. *JCAP* **11,** 020. arXiv: 2307.04691 [hep-ph] (2023).
36. Ai, W.-Y. & Drewes, M. Schwinger effect and false vacuum decay as quantum-mechanical tunneling of a relativistic particle. *Phys. Rev. D* **102,** 076015. arXiv: 2005.14163 [hep-th] (2020).
37. Griffiths, D. J. & Schroeter, D. F. *Introduction to Quantum Mechanics* 3rd ed. (Cambridge University Press, 2018).

38. Callan, C. G. & Coleman, S. Fate of the false vacuum. II. First quantum corrections. *Phys. Rev. D* **16,** 1762–1768. https://link.aps.org/doi/10.1103/PhysRevD.16.1762 (6 Sept. 1977).
39. Kibble, T. W. B. Topology of Cosmic Domains and Strings. *J. Phys. A* **9,** 1387–1398 (1976).
40. Kolb, E. W. & Turner, M. S. *The Early Universe* ISBN: 978-0-429-49286-0, 978-0-201-62674-2 (Taylor and Francis, May 2019).
41. Vilenkin, A. Gravitational Field of Vacuum Domain Walls and Strings. *Phys. Rev. D* **23,** 852–857 (1981).
42. Coleman, S. R. & De Luccia, F. Gravitational Effects on and of Vacuum Decay. *Phys. Rev. D* **21,** 3305 (1980).
43. Carroll, S. M. *Spacetime and Geometry: An Introduction to General Relativity* (Pearson, San Francisco, USA, 2003).
44. Brandenberger, R. H., Danos, R. J., Herná ndez, O. F. & Holder, G. P. The 21 cm signature of cosmic string wakes. *Journal of Cosmology and Astroparticle Physics* **2010,** 028–028. https://doi.org/10.1088%2F1475-7516%2F2010%2F12%2F028 (Dec. 2010).
45. Lopez, A. M., Clowes, R. G. & Williger, G. M. Investigating ultra-large large-scale structures: potential implications for cosmology. *Phil. Trans. Roy. Soc. Lond. A* **383,** 20240029. arXiv: 2409.14894 [astro-ph.CO] (2025).
46. Lopez, A. M., Clowes, R. G. & Williger, G. M. A Giant Arc on the Sky. *Mon. Not. Roy. Astron. Soc.* **516,** 1557–1572. arXiv: 2201.06875 [astro-ph.CO] (2022).
47. Lopez, A. M., Clowes, R. G. & Williger, G. M. A Big Ring on the sky. *JCAP* **07,** 055. arXiv: 2402.07591 [astro-ph.CO] (2024).
48. Agazie, G. *et al.* The NANOGrav 15 yr Data Set: Evidence for a Gravitational-wave Background. *Astrophys. J. Lett.* **951,** L8. arXiv: 2306.16213 [astro-ph.HE] (2023).
49. Martin, X. & Vilenkin, A. Gravitational wave background from hybrid topological defects. *Phys. Rev. Lett.* **77,** 2879–2882. arXiv: astro-ph/9606022 (1996).
50. Martin, X. & Vilenkin, A. Gravitational radiation from monopoles connected by strings. *Phys. Rev. D* **55,** 6054–6060. arXiv: gr-qc/9612008 (1997).
51. Leblond, L., Shlaer, B. & Siemens, X. Gravitational Waves from Broken Cosmic Strings: The Bursts and the Beads. *Phys. Rev. D* **79,** 123519. arXiv: 0903.4686 [astro-ph.CO] (2009).
52. Buchmuller, W., Domcke, V., Murayama, H. & Schmitz, K. Probing the scale of grand unification with gravitational waves. *Phys. Lett. B* **809,** 135764. arXiv: 1912.03695 [hep-ph] (2020).
53. Wang, J.-C., Wang, S.-J. & Yuwen, Z.-Y. Gravitational waves from vacuum bubbles: Ultraviolet dependence on wall thickness. *Phys. Rev. D* **112,** 016022. arXiv: 2503.00939 [gr-qc] (2025).
54. Kibble, T. W. B. Some Implications of a Cosmological Phase Transition. *Phys. Rept.* **67,** 183 (1980).
55. Blasi, S. & Mariotti, A. QCD axion strings or seeds? *SciPost Phys.* **18,** 016. arXiv: 2405.08060 [hep-ph] (2025).